HHS Public Access
Author manuscript
Cell Rep Phys Sci. Author manuscript; available in PMC 2024 January 18.

Published in final edited form as:
Cell Rep Phys Sci. 2023 July 19; 4(7): . doi:10.1016/j.xcrp.2023.101459.

Structure-function-guided design of synthetic peptides with anti-infective activity derived from wasp venom

Andreia Boaro[1,2,3,4,7], **Lucía Ageitos**[1,2,3,5,7], **Marcelo Der Torossian Torres**[1,2,3], **Esther Broset Blasco**[1,2,3], **Sebahat Oztekin**[1,2,3,6], **Cesar de la Fuente-Nunez**[1,2,3,8,*]

[1]Machine Biology Group, Departments of Psychiatry and Microbiology, Institute for Biomedical Informatics, Institute for Translational Medicine and Therapeutics, Perelman School of Medicine, University of Pennsylvania, Philadelphia, PA 19104, USA

[2]Departments of Bioengineering and Chemical and Biomolecular Engineering, School of Engineering and Applied Science, University of Pennsylvania, Philadelphia, PA 19104, USA

[3]Penn Institute for Computational Science, University of Pennsylvania, Philadelphia, PA 19104, USA

[4]Present address: Centro de Ciências Naturais e Humanas, Universidade Federal do ABC, Santo André, São Paulo 09210-580, Brazil

[5]Present address: CICA - Centro Interdisciplinar de Química e Bioloxía, Departamento de Química, Facultade de Ciencias, Universidade da Coruña, 15008 A Coruña, Spain

[6]Present address: Faculty of Engineering, Department of Food Engineering, Bayburt University, Bayburt 69000, Turkey

[7]These authors contributed equally

[8]Lead contact

SUMMARY

Antimicrobial peptides (AMPs) derived from natural toxins and venoms offer a promising alternative source of antibiotics. Here, through structure-function-guided design, we convert two natural AMPs derived from the venom of the solitary eumenine wasp *Eumenes micado* into α-helical AMPs with reduced toxicity that kill Gram-negative bacteria *in vitro* and in a preclinical

[*]Correspondence: cfuente@upenn.edu.

AUTHOR CONTRIBUTIONS

M.D.T.T. and C.d.l.F.-N. conceived the idea and designed and supervised the project. A.B., L.A., and M.D.T.T. conducted structural, mechanism of action, synergy, resistance development, and antimicrobial characterization *in vitro* and *in vivo*. S.O. conducted antimicrobial assays *in vitro*. E.B.B. conducted cytotoxicity experiments. A.B., L.A., M.D.T.T., and C.d.l.F.-N. wrote the first draft of the article. All the authors revised the final manuscript. C.d.l.F.-N. provided the funding.

DECLARATION OF INTERESTS

A provisional patent application has been filed on the de la Fuente Lab's related work (ID number 23-10379). C.d.l.F.-N. provides consulting services to Invaio Sciences and is a member of the scientific advisory boards of Nowture S.L. and Phare Bio. The de la Fuente Lab has received research funding or in-kind donations from United Therapeutics, Strata Manufacturing PJSC, and Procter & Gamble, none of which were used in support of this work. C.d.l.F.-N. is on the advisory board of *Cell Reports Physical Science*.

SUPPLEMENTAL INFORMATION

Supplemental information can be found online at https://doi.org/10.1016/j.xcrp.2023.101459.

Author Manuscript
Author Manuscript
Author Manuscript

mouse model. To identify the sequence determinants conferring antimicrobial activity, an alanine scan screen and strategic single lysine substitutions are made to the amino acid sequence of these natural peptides. These efforts yield a total of 34 synthetic derivatives, including alanine substituted and lysine-substituted sequences with stabilized α-helical structures and increased net positive charge. The resulting lead synthetic peptides kill the Gram-negative pathogens *Escherichia coli* and *Pseudomonas aeruginosa* (PAO1 and PA14) by rapidly permeabilizing both their outer and cytoplasmic membranes, exhibit anti-infective efficacy in a mouse model by reducing bacterial loads by up to three orders of magnitude, and do not readily select for bacterial resistance.

Graphical Abstract

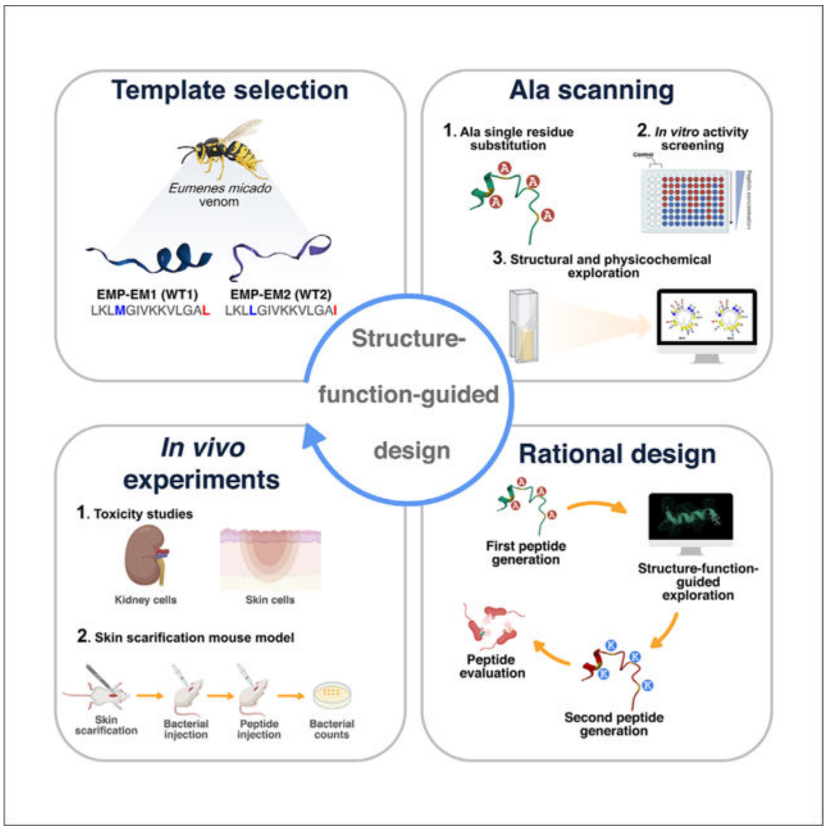

Antimicrobial peptides (AMPs) derived from natural venoms and toxins are a promising alternative to conventional antibiotics. Here, Boaro, Ageitos, et al. use a structure-function-guided design to convert two natural AMPs derived from the venom of the solitary eumenine wasp *Eumenes micado* into potent AMPs with reduced toxicity that kill Gram-negative bacteria *in vitro* and in a preclinical mouse model.

INTRODUCTION

Drug-resistant bacterial infections are a serious public health problem worldwide, as they are responsible for more than 65% of all cases of infection and lead to ~35,000 deaths in the United States annually.[1] The lack of antibiotics that can be used to treat these infections indicates the urgent need for new antimicrobial agents capable of eradicating bacterial infections.[2]

Venoms are an exciting new source of potential drugs and are being explored for antibiotic discovery.[3–7] Specifically, antimicrobial peptides (AMPs) have been found to be present in venoms or toxins.[3–10] AMPs are a promising alternative to conventional antibiotics as they can kill bacteria by penetrating through their membranes via non-specific membrane-related mechanisms of action. Either AMPs do not induce bacterial resistance or, if resistance occurs, it takes longer to develop than it does with conventional antibiotics.[2,11] Examples of AMPs from venoms include mastoparans EMP-EM1 (WT1, LKLMGIVKKVLGAL; Table 1) and EMP-EM2 (WT2, LKLLGIVKKVLGAI; Table 1), both of which are linear, cationic, amphipathic, and α-helical natural peptides extracted from the venom of the solitary eumenine wasp *Eumenes micado* (Figure 1A).[12] In addition to their antimicrobial and leishmanicidal activities, these peptides cause the degranulation of rat peritoneal mast cells.[12] However, WT1 and WT2 were also reported to have hemolytic activity for human and mouse erythrocytes at a concentration of 10^{-4} mol L^{-1},[12] preventing their application to human infections. Here, WT1 and WT2 were used as templates for the structure-function-guided rational design of analogs with fine-tuned structural and physicochemical properties. Compared with their parent peptides, the new synthetic analogs were less cytotoxic for human cells and presented increased antimicrobial activity against Gram-negative and Gram-positive pathogenic bacteria both *in vitro* and in animals.

RESULTS AND DISCUSSION

Mutational scan of peptide sequences to understand structure and function

The alanine (Ala) residue is extensively used in site-directed mutagenesis to evaluate the contribution of amino acid residues to the stability, structure, and activity of proteins and peptides. This amino acid residue presents the smallest aliphatic and chemically inert side chain, which preserves the distance between neighboring residues and does not interfere with intramolecular or intermolecular interactions.[3] Thus, we performed Ala screenings of both wild-type peptides (WT1 and WT2), generating 26 Ala-substituted synthetic derivatives, to assess the contribution of the side chain of each amino acid residue to the biological activities of the peptides (Figure 1A).

First, the physicochemical properties were theoretically determined. Normalized hydrophobicity, normalized hydrophobic moment, net positive charge, propensity to aggregate *in vitro*, and amphiphilicity index were determined by reference to the Database of Antimicrobial Activity and Structure of Peptides (DBAASP V3.0)[13] using the Eisenberg and Weiss hydrophobicity scale for all Ala-Scan (A^1-1 to A^{14}-1 and A^1-2 to A^{14}-2) and WT1 and WT2 peptides (Table 1).[14] The ratio of polar-to-non-polar amino acid residues and the helical wheels were determined using the HeliQuest webserver[15] for all peptides (Table 1; Figure S1). The normalized hydrophobicity and hydrophobic moment of all Ala-Scan and wild-type peptides ranged from −0.34 to −0.60 and from 0.29 to 0.45, respectively (Table 1), which is within the range of other known AMPs.[13] The hydrophobicity-related properties of peptides correlate with their antimicrobial activity as they are predictive of how peptides will interact with the lipid components of the bacterial membrane. The Ala-Scan derivatives

A^{12}-1, A^{2}-2, A^{5}-2, A^{8}-2, A^{9}-2, and A^{12}-2 exhibited higher values of propensity to aggregate *in vitro* (102.82, 85.50, 94.76, 83.03, 108.91, and 177.88, respectively) compared with WT1 and WT2 (15.42 and 34.76, respectively; Table 1). High values of propensity to aggregate *in vitro* are usually associated with decreased physical stability and antimicrobial activity, as well as increased cytotoxicity.[16]

In addition, most Ala-Scan derivatives presented an amphiphilicity index of 0.79 (Table 1). Because the values for the amphiphilicity index were higher than zero, all peptides showed helical structural stability at the membrane-water interface.[17] Next, we tested WT1, WT2, and their Ala-Scan derivatives for activity against the Gram-negative bacteria *Escherichia coli* ATCC 11775 and *Pseudomonas aeruginosa* strains PAO1 and PA14, as well as the Gram-positive bacterial strain *Staphylococcus aureus* ATCC 12600, based on their minimal inhibitory concentration (MIC) values (Figures 1B and S2). We performed minimal bactericidal concentration (MBC) experiments, which showed that the peptides killed the bacterial cells at the observed MIC conditions. Thus, we confirmed that the MIC and MBC values were the same by counting the colony-forming units (CFUs) after 21 h of incubation at 37°C.

WT1 and WT2 sequences are amphipathic, and, similarly to other mastoparans, they are α-helical in the presence of helix-inducing solvents.[12] To analyze the contribution of each residue's side chain to the helical structure, we performed circular dichroism (CD) experiments. In each case, the helical fraction (f_H) was determined from the negative band at 222 nm in a mixture of 2,2,2-trifluoroethanol (TFE) and water (TFE: water, 3:2, v/v) and in water alone (Table 1, and Figures 1C and 1D). We chose a TFE:water (3:2, v/v) solution because it is extensively used to study peptide secondary structure; this solution induces helical conformation in peptides by promoting dehydration and, consequently, intramolecular hydrogen bond formation.[18,19] All Ala-Scan derivatives were unstructured in water ($0.04 \le f_H \le 0.15$) but presented a helical structure in TFE:water ($0.22 \le f_H \le 0.44$), except peptide A^{11}-1, which was unstructured in both water and TFE:water. This common feature of small amphipathic cationic AMPs, known as the helical-coil transition,[20] occurs at hydrophilic-hydrophobic interfaces (Table 1; Figures 1C and 1D).

WT1 presented antimicrobial activity with MICs of 8 μmol L^{-1} for *E. coli* ATCC 11775 and 16 μmol L^{-1} for *S. aureus* ATCC 12600, and MICs of 32 μmol L^{-1} for *P. aeruginosa* PAO1 and PA14 (Figures 1B and S2). WT2 was active with MICs of 16 μmol L^{-1} for *E. coli* ATCC 11775, 32 μmol L^{-1} for *S. aureus* ATCC 12600 and *P. aeruginosa* PAO1, and 64 μmol L^{-1} for *P. aeruginosa* PA14 (Figures 1B and S2). Ala-Scan screening studies revealed that, when glycine (Gly) residues were replaced by Ala in the hydrophilic face of WT1 and WT2 sequences at positions 5 and 12 (Figure 1E), the predicted normalized hydrophobicity and observed helicity of the modified peptides increased compared with those of the wild-type peptides (Table 1; Figures 1C and 1D). The Gly residue presents the less hindered side chain (one hydrogen atom), thus leading to a high degree of freedom for the peptide, allowing different conformational intermediates, including helical steps.

The antimicrobial activities of A^{5}-1, A^{12}-1, A^{5}-2, and A^{12}-2 were significantly increased against *E. coli* ATCC 11775 and *S. aureus* ATCC 12600 (Figures 1B, S2A, and S2B).

Synthetic peptide A^5-1 was up to 4-fold more active against *E. coli* ATCC 11775 and *S. aureus* ATCC 12600 than WT1, with an MIC of 4 μmol L^{-1} for both bacterial strains. Peptide A^5-2 was 4-fold more active against *E. coli* ATCC 11775 and 8-fold more active against *S. aureus* ATCC 12600 compared with WT2, with MICs of 4 μmol L^{-1} for both bacterial strains (Figures 1B, S2A, and S2B). A^{12}-1 presented an MIC of 2 μmol L^{-1} for *E. coli* ATCC 11775 and *S. aureus* ATCC 12600, 4- and 8-fold higher than WT1, respectively. A^{12}-2 was 4-fold more active against *E. coli* ATCC 11775 and 16-fold more active against *S. aureus* ATCC 12600 than WT2, with MICs of 4 and 2 μmol L^{-1}, respectively (Figures 1B, S2A, and S2B).

When the Met residue at position 4 of the WT1 was substituted by Ala (Figure 1E), the resulting peptide, A^4-1, presented a higher helical fraction value and increased antimicrobial activity against *E. coli* ATCC 11775 (MIC = 4 μmol L^{-1}), and *S. aureus* ATCC 12600 (MIC = 8 μmol L^{-1}) compared with WT1 (Table 1; Figures 1B, 1C, S2A, and S2B). The α helix structure of A^4-1 was stabilized because Ala has the highest helical propensity (0 kcal mol^{-1}) compared with all other amino acids, whereas Met has a lower helical propensity (0.24 kcal mol^{-1}) compared with Ala.[21] Replacement of Leu at the interface between the hydrophilic and hydrophobic faces (position 4; Figure 1E) and one helical step from the charged residue lysine (Lys) (position 8; Figure 1E) of WT2 by Ala stabilized the hydrophobic face, increased the helicity, and improved the antimicrobial activity of A^4-2 against *E. coli* ATCC 11775 and *S. aureus* ATCC 12600 (Table 1; Figures 1B, 1D, S2A, and S2B). The insertion of Ala within the hydrophilic face of WT1 and WT2 (positions 4, 5, and 12, red arrows; Figure 1E) increased antimicrobial activity and stabilized the α-helical structure. Conversely, structural modifications of the hydrophobic face of WT1 and WT2 (positions 3, 6, 11, and 14, blue arrows, Figure 1E) decreased antimicrobial activity (Figures 1B and S2).

Torres et al. obtained similar results with an Ala-Scan screening of the mastoparan peptide polybia-CP, isolated from the venom of a tropical wasp species. Polybia-CP showed enhanced antibacterial activity upon Ala substitutions in the hydrophilic face or at the interface between the hydrophobic and hydrophilic faces of the peptide.[3] In addition, modifications at the hydrophobic face of polybia-CP also decreased antimicrobial activity, as observed for WT1 and WT2.[3] The presence of the hydrophobic amino acid Ile at the interface between the hydrophilic and hydrophobic faces of WT1 and WT2 (position 6, Figure 1E) was important for their antimicrobial activity since A^6-1 and A^6-2 presented lower activity (higher MIC values) against *S. aureus* ATCC 12600 and *P. aeruginosa* PAO1 and PA14 compared with both wild-type peptides (Figures 1B and S2B–S2D). Ala substitutions of Leu at positions 3, 11, and 14 of WT1, and positions 3 and 11 of WT2, also resulted in a loss of activity (Figures 1B, 1E, and S2), showing that hydrophobicity was important for the antimicrobial activity of these peptides. A^3-1, A^{11}-1, and A^{14}-1 presented lower values of helical fraction compared with WT1, suggesting a relationship between helicity and activity; however, this relationship was not observed for A^3-2 or A^{11}-2 (Table 1; Figures 1B–1D). Moreover, the residues at the end of the sequence, Leu for WT1 and Ile for WT2, were important for the antimicrobial activity of these natural peptides (Figures 1B, 1D, and S2).

Collectively, the results obtained by the Ala-Scan screening revealed a correlation between helicity and antimicrobial activity, especially for WT1-derived Ala-Scan peptides. The exception was A^1-1, as the replacement of Leu by Ala in the hydrophilic face of WT1 (position 1, Figure 1E) resulted in increased activity against all bacteria tested (MIC = 4 μmol L^{-1} for *E. coli* ATCC 11775, 8 μmol L^{-1} for *S. aureus* ATCC 12600, and 16 μmol L^{-1} for *P. aeruginosa* PAO1 and PA14; Figure S2) without increasing the helical fraction value of A^1-1 in relation to WT1 (Table 1; Figure 1C). For the WT2 derivatives, the correlation between helicity and activity was not clear, since all WT2-derived Ala-Scan peptides had higher helical fraction values compared with WT2 (Table 1). To further investigate the physicochemical and structural aspects influencing the antimicrobial activity of these natural peptides, we decided to design new derivatives of WT1 and WT2 (Table 2).

Structure-function-guided design of a new generation of synthetic peptides

Since the Ala-substituted analogs were not significantly more active than the templates, we decided to go back to the templates and assess how to tune them in order to increase their antimicrobial activity while preserving their tendency to structure helically. To achieve this, we designed a second generation of WT1 and WT2 peptides with single Lys substitutions, yielding six synthetic derivatives. Lys was selected given its tendency to lead to increased antimicrobial activity while not increasing cytotoxicity in sequences derived from venoms.[3,4,6,7,22–25] Lys residues were used instead of arginine (Arg) because Arg is more likely to increase the toxicity of short amphipathic peptides such as the EMP-EM templates.[26] We placed the single substitutions in positions that were expected to lead to analogs with higher amphipathicity and lower *in vitro* aggregation tendencies (Table 2), properties that proved to be important for the antimicrobial activity of this peptide family. To explore the two only distinguishing amino acid residues between WT1 (Met and Leu) and WT2 (Leu and Ile) (positions 4 and 14), we synthesized derivatives L^4-1 and I^{14}-1.

First, the physicochemical properties (Table 2) and helical wheel projections (Figure S3) of all new derivatives were predicted using DBAASPDBAASP[80] and HeliQuest, respectively.[13–15] The second-generation derivatives K^{12}-1, K^{13}-1, K^{10}-2, and K^{13}-2 presented lower values of propensity to aggregate *in vitro* (1.76, 1.77, 8.22, and 8.15, respectively, Table 2) compared with WT1, WT2, or Ala-Scan analogs (Table 1). These low values of propensity to aggregate *in vitro* are related to the hydrophobic balance of the peptide, which directly affects its propensity to interact with lipid membranes and, consequently, its antimicrobial activity and cytotoxicity.[16] Moreover, the second-generation derivatives showed a higher value of amphiphilicity index of 1.05 in relation to derivatives WT1, WT2, and Ala-Scan derivatives (except I^{14}-1 and L^4-1), indicating a gain in helical structural stability at the membrane-water interface (Tables 1 and 2). All eight derivatives from the second generation were synthesized and tested against the pathogenic bacteria *E. coli* ATCC 11775, *S. aureus* ATCC 12600, and *P. aeruginosa* PAO1 and PA14 (Figures 2A and S4). CFU counts of bacteria after 21 h of incubation at 37°C were used to determine the minimum bactericidal concentrations (MBCs). The secondary structures of this second generation of peptides were analyzed by CD spectroscopy measurements in TFE:water (3:2 v/v) and water (Figure 2B), and the helical fraction values were also calculated (Table 2). All derivatives were random coils in water and presented a higher f_H value in TFE:water compared with WT1 and WT2, except for K^{13}-1, which adopted a random coil in water and in TFE:water (Figure 2B), showing that the Ala residue in position 13 was important for the helical structure of WT1. On the contrary, this random-coil structure in water and in TFE:water was not observed for WT2 when we substituted the Ala residue in position 13 by a Lys residue (K^{13}-2).

Exploration of derivatives I^{14}-1 and L^4-1 showed that I^{14}-1 had a higher helical fraction value than WT1, but it was more active than WT1 only against *P. aeruginosa* PAO1 (Table 2, Figures 2A, 2B, and S4A). L^4-1 presented a lower predicted normalized hydrophobicity and higher values of helical fraction (0.88) and normalized hydrophobic moment compared with A^4-1 or WT1 (Tables 1 and 2). Despite its higher helicity, L^4-1 showed no significant improvement in activity compared with A^4-1. As previously discussed, when Gly at position 12 of WT1 was replaced by Ala, the resulting analog, A^{12}-1, was more active than WT1 against *E. coli* ATCC 11775 and *S. aureus* ATCC 12600 (MIC = 2 μmol L^{-1}) but showed no significant improvement in activity against *P. aeruginosa* strains PAO1 and PA14 compared with WT1 (Figure 1B and S2).

To further explore the effectiveness of these peptides, particularly against Gram-negative bacteria, a Lys residue was used to increase the positive net charge and decrease the flexibility and hydrophobicity of the WT1 and WT2 sequences. Gly was replaced by Lys at position 12 of the WT1 sequence, leading to derivative K^{12}-1, which, compared with WT1, had a higher helical fraction in TFE:water (0.62, Table 2) and was 8-fold more active against *P. aeruginosa* PAO1, 4-fold more active against *S. aureus* ATCC 12600 and *P. aeruginosa* PA14, and 2-fold more active against *E. coli* ATCC 11775 (Figures 2A and S4). Lys-for-Gly substitutions in mastoparans usually increase antimicrobial activity, mainly because this family of peptides is known for their secondary-structure-dependent antimicrobial activity and Lys is a positively charged residue that stabilizes the secondary structure.[3] On the contrary, Gly is highly flexible, favoring intermolecular interactions and destabilizing the secondary structure.[3] Interestingly, analog K^{13}-1, which presented a random-coil secondary structure in water and TFE:water (Figure 2B), was 4-fold more active against *P. aeruginosa* PAO1 (MIC of 8 μmol L^{-1}) and 2-fold more active against *E. coli* ATCC 11775 (MIC of 4 μmol L^{-1}) and *P. aeruginosa* PA14 (MIC of 16 μmol L^{-1}) than WT1 (Figures 2A and S4). A positive charge was added to this derivative at the interface between the hydrophilic and hydrophobic faces when the Ala residue, at position 13 of the WT1 sequence, was replaced by Lys (Figure S3). On the other hand, such modification at the interface caused an 8-fold decrease in the activity of K^{13}-1 against *S. aureus* ATCC 12600, increasing the MIC to 128 μmol L^{-1} (Figures 2A and S4B).

To assess the effect of a positive charge at the N-terminal extremity of the WT2 sequence, a Leu residue was substituted by Lys, leading to the synthetic derivative K^1-2 (Table 2). Such replacement at the N-terminal extremity stabilized the α helix structure, and K^1-2 was up to 4-fold more active against Gram-negative bacteria than WT2 (Table 2; Figures 2A and S4). In addition, Ile and Ala residues were substituted by Lys at the interface between the hydrophilic and hydrophobic faces of WT2, yielding derivatives K^6-2 and K^{13}-2, respectively. K^6-2 was 2-fold less active against *E. coli* ATCC 11775 than WT2 and was not active against *S. aureus* ATCC 12600 at any of the concentrations tested (Figures 2B and S4). These results confirm the importance for its antimicrobial activity of the Ile residue at these positions within the WT2 sequence, as previously observed for A^6-2, since this derivative also lost activity when Ile was replaced by Ala (Figures 1B, 1E, and S2). K^{13}-2 exhibited 2-fold decreased activity against *S. aureus* ATCC 12600; however, this peptide presented up to 8-fold greater activity against all tested Gram-negative bacteria compared with WT2, with MICs of 4 μmol L^{-1} for *E. coli* ATCC 11775 and *P. aeruginosa* PAO1, and 16 μmol L^{-1} for *P. aeruginosa* PA14, which may derive from its high helical fraction (0.89, Table 2; Figures 2A, 2B, and S4). Finally, to test the effect of inserting a positive charge on the hydrophobic face of WT2, Val was replaced by Lys, yielding K^{10}-2. Peptide K^{10}-2 showed greater helicity; 4-fold higher antimicrobial activity against *E. coli* ATCC 11775, and *S. aureus* ATCC 12600; and 8-fold higher antimicrobial activity against *P. aeruginosa* PAO1 and PA14 compared with WT2, with MICs of 4 μmol L^{-1} for *E. coli* ATCC 11775 and *P. aeruginosa* PAO1, and 8 μmol L^{-1} for *S. aureus* ATCC 12600 and *P. aeruginosa* PA14 (Table 2; Figures 2A, 2B, and S4). Thus, replacing residues from the original sequence with a Lys residue at strategic positions of the WT1 and WT2 sequences, which increased the net positive charge of these peptides, significantly improved their antimicrobial activity against Gram-negative bacteria (except for K^6-2), although it decreased the activity of K^{13}-1, K^6-2, and K^{13}-2 against *S. aureus* ATCC 12600 (Figures 2A and S4). Nonetheless, K^{12}-1 and K^{10}-2 were more active against all tested bacteria compared with their corresponding templates, WT1 and WT2 (Figures 2A and S4).

Mechanism of action, synergy, and evolution of bacterial resistance

Since AMPs, such as mastoparans, generally establish the first contact with the bacterial cell membrane by electrostatic and hydrophobic interactions, these peptides can act through different mechanisms of action (MoAs) and any structural modification can affect their MoAs.[8,27,28] For MoA studies, we selected *P. aeruginosa* PAO1 as a model bacterial strain, because of its medical importance as a multidrug-resistant pathogen,[29] and the following peptides: (1) both templates WT1 and WT2; (2) K^{12}-1 for being the most active peptide from WT1 family against Gram-negative and Gram-positive bacterial strains (Figures 2A and S4); (3) K^{13}-1 for its activity against the Gram-negative strains tested and its random-coil secondary structure (Table 2; Figure 2B); (4) K^{13}-2 also for its activity against the Gram-negative strains tested and for presenting the highest value of helical fraction among all studied peptides (Table 2); and (5) polymyxin B (PMB) for being a well-known membrane-disrupting peptide.[30]

To assess whether these peptides permeabilize bacterial outer membranes, we used the fluorescent probe (1-(*N*-phenylamino)-naphthalene (NPN). In aqueous environments, NPN emits weak fluorescence and can only permeate bacterial outer membranes when those membranes are damaged.[31] When this probe interacts with the lipidic environment of damaged outer membranes, it emits fluorescence at increased intensity, indicating that the membrane has been permeabilized by the peptide (Figure 3A).[31] The NPN assay showed that all tested peptides permeated the outer membrane of *P. aeruginosa* PAO1, as observed for PMB (Figure 3B). To evaluate whether these peptides depolarize the cytoplasmic membrane of *P. aeruginosa* PAO1, we utilized the probe 3,3′-dipropylthiadicarbocyanine iodide ($DiSC_3$-5). $DiSC_3$-5 is a potentiometric probe that accumulates in cytoplasmic membranes and aggregates at high concentrations, causing fluorescence quenching. When the cytoplasmic membrane is destabilized, $DiSC_3$-5 migrates to the cytoplasm or to the external environment, emitting increased fluorescence intensity (Figure 3C).[31] The $DiSC_3$-5 assay revealed that all tested peptides depolarized the cytoplasmic membrane of *P. aeruginosa* PAO1 more efficiently than PMB (Figure 3D). K^{12}-1 was the most efficient peptide in destabilizing the outer and cytoplasmic membranes of *P. aeruginosa* PAO1 compared with other peptides, corresponding to its high antimicrobial activity against all tested bacteria (Figures 2A, 3B, and 3D). The random-coil peptide K^{13}-1, such as all the tested α-helical peptides, also permeated the outer membrane and depolarized the cytoplasmic membrane of *P. aeruginosa* PAO1 (Figures 3B and 3D). This was an interesting observation that revealed that the mechanism of action of these peptides was not entirely driven by their secondary structure.

On the other hand, K^{13}-2, the peptide with the highest helical fraction value among all second-generation derivatives (Table 2), was the least efficient in destabilizing the outer and cytoplasmic membranes, further demonstrating that the MoAs of these peptides do not depend entirely on their secondary structure (Figures 3B and 3D).

To evaluate whether WT1, WT2, K^{12}-1, and K^{13}-1 can interact synergistically with antibiotics with different MoAs, a synergy assay was performed (Figure 3E). First, seven antibiotics (i.e., ciprofloxacin, metronidazole, ofloxacin, gentamicin, PMB, erythromycin, and chloramphenicol) were tested for activity against *P. aeruginosa* PAO1 (Figure S6). As metronidazole and chloramphenicol were not active against *P. aeruginosa* PAO1 at the highest concentration tested (128 μmol L^{-1}; Figure S6), the other five of these antibiotics were selected for further testing. These five antibiotics were diluted using the microdilution technique at concentrations ranging from 2- to 0.03-fold MIC and combined with WT1, WT2, K^{12}-1, and K^{13}-1 with the same range of concentrations (Figure S7). No synergistic effect was observed when these peptides were combined with any of the five commercial antibiotics (Figures 3E and S7). Clarifying the synergistic interactions (or lack thereof) of antibiotic combinations requires a deep understanding about the MoAs underlying the biological activity of each drug. Our MoA studies revealed that these peptides can rapidly kill Gram-negative bacteria such as *P. aeruginosa* PAO1 by efficiently permeabilizing their outer and cytoplasmic membranes (Figures 3B and 3D). However, additional intra-cellular modes of action involved in the antimicrobial activity of these peptides have not yet been characterized and warrant further studies. Based on the mechanistic results obtained here, we propose that these peptides can effectively kill Gram-negative bacteria at the membrane level. However, these membrane-targeting mechanisms of the peptides do not necessarily lead to synergy with conventional antibiotics. A deeper understanding of the specific modes of action involved in the antimicrobial activity of these peptides is needed.

Although numerous papers have been published describing the synergistic effects between membrane-permeating peptides and antibiotics whose targets are intracellular, this tendency is not necessarily widespread.[32–38] For example, studies have addressed the lack of synergy between membrane-disrupting cationic AMPs and conventional antibiotics.[32–34,39,40] Giacometti et al. reported that magainin II synergized with β-lactam antibiotics, but no synergy was observed when magainin II was combined with other classical antibiotics.[32–34]

On the other hand, Ulvatne et al. reported a lack of synergy when certain synthetic peptides were combined with β-lactam antibiotics. The authors suggested that their peptides interacted with bacterial membranes by alternative modes of action independently of pore formation.[40]

The lowest fractional inhibitory concentration indices (FICIs) were obtained when PMB was combined with WT1 (0.7), WT2 (0.5), K^{12}-1 (0.7), or K^{13}-1 (0.6) (Figures 3E and S7), indicating an additive effect for each of these peptides combined with PMB against *P. aeruginosa* PAO1. An additive effect is equivalent to the sum of the effects of the individual components; thus, these peptides may act through the same MoAs as PMB. PMB acts via a self-promoted uptake pathway by binding to negatively charged phosphate groups on the lipopolysaccharide in the outer membrane of Gram-negative bacteria.[30] PMB destabilizes the outer membrane and permeabilizes it and can penetrate the cytoplasmic membrane by binding to phospholipids, causing lethal leakage of cytoplasmic components.[30] An additive effect for the combination of WT1, WT2, K^{12}-1, or K^{13}-1 and PMB is in agreement with the results of our MoA studies. Thus, the activity of these peptides does not synergize with that of PMB, since these peptides can permeate the outer membrane and depolarize the cytoplasmic membrane more efficiently than PMB (Figures 3B and 3D). As both templates are produced within the same venom, we hypothesized that WT1 and WT2 act synergistically in the venom mixture. Therefore, WT1 and WT2 were tested in combination at different concentrations against the pathogenic strain *P. aeruginosa* PAO1. We observed an additive effect (FICI = 0.7), as previously obtained by the combinations of the template peptides and PMB (Figure S7).

To evaluate whether WT1, K^{12}-1, and K^{13}-1 select for pathogen resistance, a resistance development assay was performed with *E. coli* JW2703 (hypermutant strain) Δ*mutS*::kan. (from the Keio collection), hereafter referred to as *E. coli* Δ*mutS* for simplicity; ciprofloxacin, a broad-spectrum second-generation fluoroquinolone that acts by inhibiting DNA replication; and PMB, a known membrane disrupting agent.[41] Ciprofloxacin was used as a positive control because it is well known to rapidly trigger resistance development in bacteria.[42–45] The strain *E. coli* JW2703 Δ*mutS*::kan was selected for the resistance development experiment because it is more relevant than wild-type *E. coli* or *P. aeruginosa* strains due to its ability to rapidly mutate, making it an excellent strain for resistance development assays as previously reported.[46] This strain is mutated in its *mutS* gene, yielding a hypermutant strain. The development of resistance in *E. coli* Δ*mutS* was assessed by monitoring changes in the MICs of WT1, K^{12}-1, K^{13}-1, and ciprofloxacin induced by increasing concentrations of treatment over 20 days (Figure 3F). Treatment with the fluoroquinolone ciprofloxacin induced bacterial resistance within 4 days from the onset of the experiment, and the MIC of ciprofloxacin increased by 1,000-fold after 18 days (Figure 3F). Conversely, the MICs of WT1, K^{12}-1, K^{13}-1, and PMB did not vary significantly over the same period. Thus, these peptides killed *E. coli* Δ*mutS* without selecting for peptide-resistant mutants (Figure 3F). Bacterial killing likely occurs through non-specific MoAs; once such peptides disrupt the outer and cytoplasmic membrane of bacteria, the cytoplasmic content leaks out, causing bacterial cell death.[47]

Cytotoxicity profile studies and *in vivo* antimicrobial activity in a mouse model

P. aeruginosa is a pathogenic bacterium that causes pneumonia and infections of the skin, the urinary tract, and the gastrointestinal tissue.[48–51] This bacterium has developed resistance to available antibiotics,[52] and antimicrobial peptides have been considered potential candidates for the treatment of these infections.[53] First, peptides WT1, WT2, one Ala-substituted analog, and the second-generation derivatives that presented potent activity against *P. aeruginosa* PAO1 (i.e., A^{14}-1, K^{12}-1, K^{13}-1, K^{10}-2, and K^{13}-2) were tested for cytotoxicity against human embryonic kidney (HEK) cells (ATCC HEK293T; Figure 4A) and primary human keratinocytes (Figure 4B). Primary human keratinocytes were used as a proxy for analyzing the toxicity of peptides in contact with the skin, and HEK cells were used in cytotoxicity assays because many antibiotics are excreted by the kidney and a requirement for promising new drugs is that they be non-nephrotoxic.[54] Peptide concentrations used in the cytotoxicity analysis ranged from 1 to 64 μmol L^{-1}, as the MICs of all tested peptides were below 64 μmol L^{-1} against all tested bacteria. When treated with the peptides WT1, WT2, and K^{12}-1 at their corresponding MIC for *P. aeruginosa* PAO1, the keratinocytes retained 70%, 86%, and 96% cell viability, respectively (Figures 4B and S4C). WT1 at its MIC showed toxicity for HEK cells, with cell viability of 75%, while WT2 and K^{12}-1 were toxic for HEK cells at 2- and 4-fold MIC, with cell viability of 13% and 65%, respectively (Figures 4A and S4C). K^{10}-2 exhibited no toxicity against keratinocytes at 8 μmol L^{-1} (with 92% of cell viability remaining) and against HEK cells at 16 μmol L^{-1} (i.e., 2- and 4-fold higher than its MIC against *P. aeruginosa* PAO1; Figures 4A, 4B, and S4C). The most promising results were obtained for K^{13}-1 and K^{13}-2 (Figures 4A and 4B). These peptides presented a low toxicity against keratinocytes at the highest concentration tested (i.e., 64 μmol L^{-1}, from 8- to 16-fold higher than their MIC, against *P. aeruginosa* PAO1; Figures 4B and S4C), thus proving a pronounced therapeutic window. K^{13}-1 was toxic for HEK cells at 4-fold MIC, and A^{14}-1 and K^{13}-2 presented no toxicity against HEK cells at any of the concentrations tested (Figures 4A and S4C). The peptides K^{13}-1 and K^{13}-2 are more cationic and amphipathic than their templates (WT1 and WT2, respectively) and the first-generation peptides. Thus, it is to be expected that there will be a weaker interaction between such peptides and eukaryotic membranes compared with bacterial membranes, since eukaryotic membranes are more hydrophobic and only slightly negatively charged.[55,56]

Therefore, based on their optimal toxicity profiles, peptides K^{12}-1, K^{13}-1, and K^{13}-2 were selected for *in vivo* studies at the safe concentrations of 16, 16, and 32 μmol L^{-1}, respectively, in a skin scarification mouse model (Figure 4C).[6,57–59] To assess peptide toxicity *in vivo*, mice were weighed before and after treatment to monitor weight variation, since variations of up to 20% are a widely used proxy of distress, morbidity, and overall toxicity.[31,60,61] We also monitored the mice for toxicity markers such as itchiness,[62,63] redness,[64] and swelling.[65,66] None of the tested peptides showed side effects or toxicity *in vivo*, indicated by no significant change in the body weight of the treated mice compared with untreated mice (Figure 4D). Skin infection was induced by administering a *P. aeruginosa* PAO1 solution at 10^7 CFU mL^{-1} on the back of mice previously scratched with a needle and treated witha single dose of peptide solutions (Figure 4C). After 2 days of treatment, K^{12}-1, K^{13}-1, and K^{13}-2 reduced bacterial quantities by 38-, 112-, and

4,600-fold, respectively, compared with the untreated control group of mice (Figure 4E). The peptide K^{13}-2 showed potent bactericidal activity *in vivo* after 2 days of treatment. After 4 days of treatment, K^{12}-1 still inhibited the proliferation of bacterial cells (i.e., showed bacteriostatic activity), while K^{13}-1 had a bactericidal effect (Figure 4E). Peptides K^{13}-1 and K^{13}-2 did not completely sterilize the infection but reduced bacterial loads by 1,050- and 13,460-fold (three and five orders of magnitude) compared with the untreated control group, respectively, with single-dose administration at low concentrations (16 and 32 μmol L^{-1}, respectively) after 4 days of treatment (Figure 4E).

To conclude, drug-resistant bacterial infections have become a serious public health problem that needs to be addressed with novel strategies. AMPs are potential candidates for new antibiotics because their use is unlikely to select for resistance due to the use of simultaneous and diverse MoAs toward different targets in bacteria.[67,68] Venoms, which serve the producing organism as a means of defense and predation, are a source of a multitude of AMPs.[4,68,69] Here, we used a structure-function-guided design approach to fine-tune the physicochemical features of EMP-EM1 (WT1) and EMP-EM2 (WT2), two mastoparan-like peptides isolated from *E. micado* wasp venom. First, we unraveled the importance of each amino acid residue to their antimicrobial activity by performing an Ala-Scan screening. We then evaluated the role of their secondary structure (α helix), net charge, and the positions of certain residues within their hydrophilic face and interface in relation to antimicrobial activity. Altogether, Ala substitutions within the hydrophobic face at positions 3, 11, and 14, and at position 6, on the interface, significantly decreased the antimicrobial activity of the peptides (Figures 1B and 1E). Conversely, Ala substitutions at positions 5 and 12 within the hydrophilic face, and at position 4 within the interface, increased the antimicrobial activity and helical fraction. When a Gly residue was replaced by Ala at positions 5 and 12 within the WT1 and WT2 sequences (Figure 1E), the degree of freedom for these peptide structures decreased, favoring the stabilization of the helical structure, which proved to be crucial for the antimicrobial activity of this class of peptides.[3] For peptide A^{4}-1, as the Met residue has a lower helical propensity value than Ala,[21] replacing Met by Ala can influence the stability of this peptide's secondary structure.

The rational design of a second generation of synthetic peptides based on Lys substitutions resulted in peptides with lower theoretical values for *in vitro* aggregation and increased amphipathicity, which were also less toxic *in vitro* (Figures 4A and 4B) and possessed increased antimicrobial activity against Gram-negative bacteria (Figure 2A), compared with their respective templates WT1 and WT2 (Figures 1B, 4A, and 4B). Conversely, peptides with positive net charge values higher than the template showed a decrease in antimicrobial activity against the Gram-positive bacterium *S. aureus*. This finding could help to lay the foundation for the future development of narrow-spectrum peptides aimed at treating Gram-negative bacteria. These Lys-substituted peptides killed bacteria by permeabilizing and depolarizing the membrane. Furthermore, no resistance to the peptides was observed to develop in a hypermutant *E. coli* strain over 20 days. Collectively, our data indicate that adding Lys to the EMP-EM derivatives leads to increased positive charge, in turn likely yielding more effective electrostatic interactions with anionic bacterial membranes.[70–73] The structure-function-guided design approach based on Lys substitutions yielded peptide K^{13}-2, which displayed increased antimicrobial activity, low toxicity against keratinocytes and HEK cells, and potent anti-infective properties *in vivo* compared with its predecessor WT2. To the best of our knowledge, this is the first time that the natural peptides EMP-EM1 and EMP-EM2 have been used as scaffolds for the rational design of optimized synthetic AMPs. Briefly, we demonstrated the ability of Ala scan screening and strategic single Lys substitutions to guide peptide design leading to AMPs with increased antimicrobial activity compared with their natural templates derived from venoms. The synthetic peptides designed here constitute active antibiotic scaffolds that warrant further development.

EXPERIMENTAL PROCEDURES

Resource availability

Lead contact—Further information and requests for resources should be directed to and will be fulfilled by the lead contact, Cesar de la Fuente-Nunez (cfuente@upenn.edu).

Materials availability—This study did not generate new unique reagents.

Data and code availability—All data reported in this paper will be shared by the lead contact upon reasonable request. This work did not generate any code.

Solid-phase peptide synthesis, purification, and analysis

Peptides were purchased from AAPPTec, and synthesized by solid-phase peptide synthesis, using a fluorenylmethyloxycarbonyl (Fmoc) strategy on rink amide resin.

CD spectroscopy

CD experiments were performed on an Aviv CD spectrometer from the Biological Chemistry Resource Center (BCRC) of the University of Pennsylvania. CD spectra were recorded in three replicates at 25°C using a 0.25-mL quartz cuvette with 1.0-mm optical path length between 260 and 190 nm at 50 nm min^{-1} and bandwidth of 0.5 nm. The concentration of all peptides was 50 μmol L^{-1} and the measurements were performed in water and in a mixture of water and TFE 3:2 after recording the respective baselines.

Bacterial strains

The strains used in this work were *E. coli* ATCC 11775, *E. coli* JW2703 (hypermutant strain) Δ*mutS*::kan. (from the Keio collection) (kindly donated by Mark Goulian), *P. aeruginosa* PAO1, *P. aeruginosa* PA14, and *S. aureus* ATCC 12600.

MIC assays

The MIC assays were performed following the microdilution method.[74] Peptide solutions of 256 μmol L^{-1} in Milli-Q sterile-filtered water were added to 96-well round-bottom plates, and a 2-fold serial dilution was performed to obtain peptide concentrations ranging from 128 to 2 μmol L^{-1}. Bacterial solutions at 5×10^5 CFU mL^{-1} in Luria-Bertani (LB) broth medium of *E. coli* ATCC 11775, *S. aureus* ATCC 12600, and *P. aeruginosa* (PAO1 and PA14) were added to the plates, and plates were incubated for 24 h at 37°C. After treatment, the optical density (OD) at 600 nm of the plates was measured on a Thermo Scientific Varioskan LUX fluorescence spectrophotometer to check bacterial growth inhibition and to compare results with those of untreated controls. Heatmaps obtained directly from OD measurements of the plates after treatment with all tested peptides and bacteria are shown in Figures S2 and S4. All MIC assays were performed in three replicates.

Bacterial killing experiments

Bacterial killing experiments to determine the MIC were performed according to Wiegand et al.[74] After 24 h of treatment, solutions corresponding to MIC and MIC/2 (identified by OD measurements) were collected and transferred to 96-well round-bottom plates, and serially diluted in 10-fold increments. Solutions were plated on LB agar plates (for *E. coli* ATCC 11775 and *S. aureus* ATCC 12600) and Pseudomonas Isolation Agar plates (for *P. aeruginosa* PAO1 and PA14), and cultures were incubated for 21 h at 37°C. Next, bacterial colonies were counted. The MBC was assessed by counting CFUs to confirm the MIC values of all peptides of this study against all bacterial strains tested. All assays were done in four replicates, including the controls.

NPN assay

The NPN assay for outer membrane permeabilization studies was performed based on the Hancock & Wong method.[75] *P. aeruginosa* PAO1 cells were grown to an OD at 600 nm of 0.5, centrifuged, and diluted ina5 mmol L^{-1} sterile-filtered buffer solution *N*-2-hydroxyethylpiperazine-*N′*−2-ethanesulfonic acid (HEPES) with pH of 7.4 for 0.4 OD mL^{-1}. Bacteria cells were washed three times with HEPES solution and centrifuged for 5 min at 10,000 rpm. Solutions of WT1, K^{12}-1, K^{13}-1, WT2, K^{13}-2, and PMB were added to a white 96-well plate at their corresponding MICs. Four microliters of a 5-mmol L^{-1} stock solution of NPN in acetone was added to all wells containing peptide solution in the dark, to avoid photophysical decomposition. The bacterial solution, previously prepared in HEPES solution, was quickly added to the plate in the dark. The plate was read immediately and then every minute for 30 min, on a Thermo Scientific Varioskan LUX fluorescence spectrophotometer with the excitation wavelength set to 350 nm and emission wavelength set to 420 nm. All assays were done in three replicates, including the controls, which consisted of only HEPES solution, HEPES solution and NPN, HEPES solution and *P. aeruginosa* PAO1, and HEPES solution with both *P. aeruginosa* PAO1 and NPN.

$DiSC_3$-5 assay

The $DiSC_3$-5 assay for cytoplasmic membrane depolarization studies was performed according to Zhang et al.[76] *P. aeruginosa* PAO1 cells were grown to an OD at 600 nm of 0.5, centrifuged, and washed with a 5-mmol L^{-1} sterile-filtered HEPES solution containing 20 mmol L^{-1} of glucose with pH of 7.2. After washing, the supernatant was removed, and a bacterial solution was prepared in 5 mmol L^{-1} of HEPES solution containing 20 mmol L^{-1} of glucose and 0.1 mol L^{-1} of KCl with pH 7.2. This bacterial solution was added to a black 96-well plate and read on the fluorescence spectrophotometer with the excitation wavelength set to 622 nm and the emission wavelength set to 670 nm. After that, 2 μL of a stock solution of $DiSC_3$-5 (0.1 mmol L^{-1} in dimethyl sulfoxide) was added in the dark, and the plate was read every minute for 20 min. Solutions of the WT1, K^{12}-1, K^{13}-1, WT2, K^{13}-2, and PMB peptides, at their corresponding MICs, were quickly added to the plate in the dark, and the plate was read immediately every minute for 60 min (until a plateau in the emission intensity was reached). After that, 5 μL of triton solution was added, and the plate was read every minute for 20 min (Figure S5). All assays were done in three replicates, including the controls, which consisted of only HEPES solution, and HEPES solution containing *P. aeruginosa* PAO1 and $DiSC_3$-5.

Synergy assays

After determining the MIC of each antibiotic and the four peptides tested (i.e., ciprofloxacin, ofloxacin, gentamicin, PMB, erythromycin, WT1, WT2, K^{12}-1, and K^{13}-1) for *P. aeruginosa* PAO1 (Figure S6), antibiotics and peptides were diluted using the microdilution technique to concentrations ranging from 2- to 0.03-fold MIC in different 96-well plates and then combined pairwise. Plates were incubated with 5 3 10^5 CFU mL^{-1} of *P. aeruginosa* PAO1 at 37°C for 24 h. All assays were done as three independent replicates. The OD at 600 nm was then measured (Figure S7), and the activity was studied using the FICI to evaluate synergy, considering FICI < 0.5 as synergistic, 0.5 < FICI < 1.0 as additive, 1.0 < FICI < 4.0 as indifferent, and FICI > 4.0 as antagonistic.[77–79]

Resistance development assays

The MIC for *E. coli* JW2703 (hypermutant strain) Δ*mutS*::kan. (from the Keio collection) was determined with peptides WT1, K^{12}-1, and K^{13}-1 and the antibiotics ciprofloxacin and polymyxin B using a bacterial solution at 5×10^5 CFU mL^{-1} in nutrient broth (NB) medium, according to the procedure described above. After treatment, the OD at 600 nm was measured and the bacterial solutions containing the minimal concentrations of peptide or antibiotic in which the bacteria grew (at least 50% of the bacterial growth of the control) were collected, diluted in NB medium (1:100), and incubated overnight at 37°C with stirring (250 rpm). The remaining volume of all chosen solutions was stored in a round bottom 96-well plate containing sterile glycerol solution (50%) at −80°C. A 96-well plate was prepared containing peptide/antibiotic solutions with concentrations ranging from 8- to 0.25-fold the MIC. All pre-inoculums were diluted in NB medium (1:100) after incubation, added to the plate, and incubated overnight at 37°C. After treatment, OD at 600 nm was measured, and bacterial solutions containing the minimal concentrations of peptide or antibiotic in which the bacteria were able to grow were collected, diluted in NB medium (1:100), and incubated overnight at 37°C with stirring. The remaining volume of all chosen solutions was stored in a round-bottom 96-well plate containing sterile glycerol solution at −80°C. This procedure was repeated until bacterial resistance was observed (20 days). All tests were performed as three independent replicates.

Cytotoxicity assays

Human embryonic kidney 293T (HEK293T) cells were maintained in Dulbecco's modified eagle medium (DMEM) supplemented with heat-inactivated 10% fetal bovine serum, and keratinocytes were maintained in Medium 154 supplemented with human keratinocyte growth supplement (HKGS, Gibco), Keratinocyte serum free medium (SFM), Combo Combination (Gibco), and with antibiotic/antimycotic solution (Gibco). Cells were seeded in 96-well tissue-culture-treated plates at a density of 5×10^4 cells per well in their respective media. HEK293T cells were then incubated for 24 h and keratinocytes for 48 h, in 5% CO_2, at 37°C for cell adhesion. After adhesion, media were replaced and supplemented with concentrations of tested peptides ranging from 64 to 1 μmol L^{-1} (or media without peptide as a control) in a final volume of 100 μL per well. After 24 h of incubation, 25 μL of activated 2,3-Bis-(2-Methoxy-4-Nitro-5-Sulfophenyl)-2*H*-Tetrazolium-5-Carboxanilide (XTT, Biotium) was added to each well and the plate was incubated for 5 h, in 5% CO_2, at 37°C. The XTT mitochondrial reduced product absorbance was measured at 460 nm and the background at 690 nm was subtracted. Cytotoxicity was determined as a percentage of the maximum value of cells without peptide compared with the minimum value of corresponding media without cells (% cell viability = 100 × [(X-MIN)/(MAX-MIN)]). Keratinocytes were purchased from the Penn Skin Biology and Diseases Resource-based Center (SBDRC).

Skin scarification mouse model

The methodology used is described in detail in Pane et al.[58] Briefly, the anti-infective activity of the peptides K^{12}-1, K^{13}-1, and K^{13}-2 against *P. aeruginosa* PAO1 in a mouse model was assessed. CD-1 female mice (6 weeks old) were used and maintained in the University Laboratory Animal Resources (ULAR) at the University of Pennsylvania (protocol 806763). Four mice per group in each condition were used in two independent replicates to ensure accuracy. Mice were anesthetized with isoflurane, weighed, and their backs were shaved. A needle was then used to damage the stratum corneum and upper layer of the epidermis of the skin, causing a superficial linear skin abrasion. Fifty microliters of a bacterial solution at 10^7 CFU mL^{-1} in phosphate-buffered saline (PBS) of *P. aeruginosa* PAO1 was inoculated over the scratch in the back of the mice. After 1 h, peptide solutions in PBS of 32 μmol L^{-1} for K^{13}-2 and 16 μmol L^{-1} for K^{12}-1 and K^{13}-1 were added to the infected area. After 2 days, mice from each group were killed and weighed, and the area of scarified skin was collected, homogenized using a bead beater for 20 min (25 Hz), and serially diluted for CFU quantification. This procedure was repeated after 4 days with mice from each group. The body weight of mice was monitored before and after 2 and 4 days of treatment to assess peptide cytotoxicity *in vivo*. The skin scarification mouse model (protocol number 806763) was revised and approved by the ULAR from the University of Pennsylvania.

Supplementary Material

Refer to Web version on PubMed Central for supplementary material.

ACKNOWLEDGMENTS

C.d.l.F.-N. holds a Presidential Professorship at the University of Pennsylvania and acknowledges funding from the Procter & Gamble Company, United Therapeutics, a BBRF Young Investigator Grant, the Nemirovsky Prize, the Penn Health-Tech Accelerator Award, and the Dean’s Innovation Fund from the Perelman School of Medicine at the University of Pennsylvania. Research reported in this publication was supported by the Langer Prize (AIChE Foundation), the National Institute of General Medical Sciences of the National Institutes of Health under award number R35GM138201, and the Defense Threat Reduction Agency (DTRA; HDTRA11 810041, HDTRA1-21-1-0014, and HDTRA1-23-1-0001). We thank Dr. Karen Pepper

for editing the manuscript and de la Fuente Lab members for insightful discussions. We thank the Fundação de Amparo à Pesquisa do Estado de São Paulo (FAPESP) for the provided grants (A.B. 2016/10585-4 and 2019/15871-3), Xunta de Galicia for a pre-doctoral fellowship 2019 co-funded with the social European funding (FSE) of the European Union (ED481A-2019/081), and Turkish Council of Higher Education (CoHE) Research Scholarship for Doctoral Studies Abroad (YOK-YUDAB/2019). We thank Dr. Mark Goulian for kindly donating

E. coli JW2703 (hypermutant strain) Δ*mutS*::kan. (from the Keio collection). Keratinocytes were purchased from the Penn Skin Biology and Diseases Resource-based Center (SBDRC) and, as a result, support for this work was also provided by the Penn Skin Biology and Diseases Resource-based Center, funded by NIH/NIAMS grant P30-AR069589 and the University of Pennsylvania Perelman School of Medicine. All figures were prepared in BioRender.com.

INCLUSION AND DIVERSITY

One or more of the authors of this paper self-identifies as an underrepresented ethnic minority in their field of research or within their geographical location. One or more of the authors of this paper self-identifies as a gender minority in their field of research. We support inclusive, diverse, and equitable conduct of research.

REFERENCES

1. Centers for Disease control and prevention Unit, C. for D.C. and P. (U. S.., (U.S.), N.C. for E.Z. and I.D., and Strategy, D. of H.Q.P.A.R.C. and S.U. (2019). Antibiotic Resistance Threats in the United States, 2019. CDC, 114.
2. Muttenthaler M, King GF, Adams DJ, and Alewood PF (2021). Trends in peptide drug discovery. Nat. Rev. Drug Discov. 20, 309–325. 10.1038/s41573-020-00135-8. [PubMed: 33536635]
3. Torres MDT, Pedron CN, Higashikuni Y, Kramer RM, Cardoso MH, Oshiro KGN, Franco OL, Silva Junior PI, Silva FD, Oliveira Junior VX, et al. (2018). Structure-function-guided exploration of the antimicrobial peptide polybia-CP identifies activity determinants and generates synthetic therapeutic candidates. Commun. Biol. 1, 221. 10.1038/s42003-018-0224-2. [PubMed: 30534613]
4. Silva ON, Torres MDT, Cao J, Alves ESF, Rodrigues LV, Resende JM, Lião LM, Porto WF, Fensterseifer ICM, Lu TK, et al. (2020). Repurposing a peptide toxin from wasp venom into antiinfectives with dual antimicrobial and immunomodulatory properties. Proc. Natl. Acad. Sci. USA 117, 26936–26945. 10.1073/pnas.2012379117. [PubMed: 33046640]
5. Pedron CN, Torres MDT, Lima JAD, Silva PI, Silva FD, Oliveira VX, and Oliveira VX (2017). Novel designed VmCT1 analogs with increased antimicrobial activity. Eur. J. Med. Chem. 126, 456–463. 10.1016/j.ejmech.2016.11.040. [PubMed: 27912176]
6. Torres MDT, Pedron CN, Araújo I, Silva PI, Silva FD, and Oliveira VX (2017). Decoralin analogs with increased resistance to degradation and lower hemolytic activity. ChemistrySelect 2, 18–23. 10.1002/slct.201601590.
7. Ageitos L, Torres MDT, and de la Fuente-Nunez C (2022). Biologically active peptides from venoms: applications in antibiotic resistance, cancer, and beyond. Int. J. Mol. Sci. 23, 15437. 10.3390/ijms232315437. [PubMed: 36499761]
8. Torres MDT, Sothiselvam S, Lu TK, and de la Fuente-Nunez C (2019). Peptide design principles for antimicrobial applications. J. Mol. Biol. 431, 3547–3567. 10.1016/j.jmb.2018.12.015. [PubMed: 30611750]
9. Torres MDT, Cao J, Franco OL, Lu TK, and de la Fuente-Nunez C (2021). Synthetic biology and computer-based frameworks for antimicrobial peptide discovery. ACS Nano 15, 2143–2164. 10.1021/acsnano.0c09509. [PubMed: 33538585]
10. Torres MDT, Melo MCR, Flowers L, Crescenzi O, Notomista E, and de la Fuente-Nunez C (2022). Mining for encrypted peptide antibiotics in the human proteome. Nat. Biomed. Eng. 6, 67–75. 10.1038/s41551-021-00801-1. [PubMed: 34737399]
11. Hall-Stoodley L, Costerton JW, and Stoodley P (2004). Bacterial biofilms: from the Natural environment to infectious diseases. Nat. Rev. Microbiol. 2, 95–108. 10.1038/nrmicro821. [PubMed: 15040259]
12. Konno K, Kazuma K, Rangel M, Stolarz-de-Oliveira J, Fontana R, Kawano M, Fuchino H, Hide I, Yasuhara T, and Nakata Y (2019). New mastoparan peptides in the venom of the solitary eumenine wasp Eumenes micado. Toxins 11, 155. 10.3390/toxins11030155. [PubMed: 30857348]

13. Gogoladze G, Grigolava M, Vishnepolsky B, Chubinidze M, Duroux P, Lefranc M-P, and Pirtskhalava M (2014). DBAASP: database of antimicrobial activity and structure of peptides. FEMS Microbiol. Lett. 357, 63–68. 10.1111/1574-6968.12489. [PubMed: 24888447]
14. Eisenberg D, Weiss RM, and Terwilliger TC (1984). The hydrophobic moment detects periodicity in protein hydrophobicity. Proc. Natl. Acad. Sci. USA 81, 140–144. 10.1073/pnas.81.1.140. [PubMed: 6582470]
15. Gautier R, Douguet D, Antonny B, and Drin G (2008). HELIQUEST: a web server to screen sequences with specific α-helical properties. Bioinformatics 24, 2101–2102. 10.1093/bioinformatics/btn392. [PubMed: 18662927]
16. Zapadka KL, Becher FJ, Gomes Dos Santos AL, and Jackson SE (2017). Factors affecting the physical stability (aggregation) of peptide therapeutics. Interface Focus 7, 20170030. 10.1098/rsfs.2017.0030.
17. Mitaku S, Hirokawa T, and Tsuji T (2002). Amphiphilicity index of polar amino acids as an aid in the characterization of amino acid preference at membrane-water interfaces. Bioinformatics 18, 608–616. 10.1093/bioinformatics/18.4.608. [PubMed: 12016058]
18. BUCK M (1998). Trifluoroethanol and colleagues: cosolvents come of age. Recent studies with peptides and proteins. Q. Rev. Biophys. 31, 297–355. 10.1017/S003358359800345X. [PubMed: 10384688]
19. Luo P, and Baldwin RL (1997). Mechanism of helix induction by trifluoroethanol: a framework for extrapolating the helix-forming properties of peptides from trifluoroethanol/water mixtures back to water. Biochemistry 36, 8413–8421. 10.1021/bi9707133. [PubMed: 9204889]
20. Lifson S, and Roig A (1961). On the theory of helix−coil transition in polypeptides. J. Chem. Phys. 34, 1963–1974. 10.1063/1.1731802.
21. Pace CN, and Scholtz JM (1998). A helix propensity scale based on experimental studies of peptides and proteins. Biophys. J. 75, 422–427. 10.1016/s0006-3495(98)77529-0. [PubMed: 9649402]
22. Freire KA, Torres MDT, Lima DB, Monteiro ML, Bezerra de Menezes RRP, Martins AMC, and Oliveira VX (2020). Wasp venom peptide as a new antichagasic agent. Toxicon 181, 71–78. 10.1016/j.toxicon.2020.04.099. [PubMed: 32360153]
23. Agbale CM, Sarfo JK, Galyuon IK, Juliano SA, Silva GGO, Buccini DF, Cardoso MH, Torres MDT, Angeles-Boza AM, De La Fuente-Nunez C, and Franco OL (2019). Antimicrobial and antibiofilm activities of helical antimicrobial peptide sequences incorporating metal-binding motifs. Biochemistry 58, 3802–3812. 10.1021/acs.biochem.9b00440. [PubMed: 31448597]
24. Oshiro KGN, Cândido ES, Chan LY, Torres MDT, Monges BED, Rodrigues SG, Porto WF, Ribeiro SM, Henriques ST, Lu TK, et al. (2019). Computer-aided design of mastoparan-like peptides enables the generation of nontoxic variants with extended antibacterial properties. J. Med. Chem. 62, 8140–8151. 10.1021/acs.jmedchem.9b00915. [PubMed: 31411881]
25. Torres MDT, Silva AF, Pedron CN, Capurro ML, de 14la 14Fuente-Nunez C, and Junior VXO (2018). Peptide design enables reengineering of an inactive wasp venom peptide into synthetic antiplasmodial agents. ChemistrySelect 3, 5859–5863. 10.1002/slct.201800529.
26. Li L, Vorobyov I, and Allen TW (2013). The different interactions of lysine and arginine side chains with lipid membranes. J. Phys. Chem. B 117, 11906–11920. 10.1021/jp405418y. [PubMed: 24007457]
27. Koehbach J, and Craik DJ (2019). The vast structural diversity of antimicrobial peptides. Trends Pharmacol. Sci. 40, 517–528. 10.1016/j.tips.2019.04.012. [PubMed: 31230616]
28. Souza B.M.d., Cabrera MPD, Gomes PC, Dias NB, Stabeli RG, Leite NB, Neto JR, and Palma MS (2015). Structure-activity relationship of mastoparan analogs: effects of the number and positioning of Lys residues on secondary structure, interaction with membrane-mimetic systems and biological activity. Peptides 72, 164–174. 10.1016/j.peptides.2015.04.021. [PubMed: 25944744]
29. Breidenstein EBM, de la Fuente-Núñez C, and Hancock REW (2011). Pseudomonas aeruginosa: all roads lead to resistance. Trends Microbiol. 19, 419–426. 10.1016/j.tim.2011.04.005. [PubMed: 21664819]

30. Allison DG, and Lambert PA (2015). In Chapter 32 - Modes of Action of Antibacterial Agents, Tang Y-W, Sussman M, Liu D, Poxton I, and Schwartzman J, eds. (Academic Press), pp. 583–598. 10.1016/B978-0-12-397169-2.00032-9.
31. Arqué X, Torres MDT, Patiño T, Boaro A, Sánchez S, and De La Fuente-Nunez C (2021). Autonomous treatment of bacterial infections in vivo using antimicrobial micro- and nanomotors. ACS Nano 16, 7547–7558. 10.1021/acsnano.1c11013.
32. Giacometti A, Cirioni O, Del Prete MS, Barchiesi F, Fortuna M, Drenaggi D, and Scalise G (2000). *In Vitro* activities of membrane-active peptides alone and in combination with clinically used antimicrobial agents against stenotrophomonas maltophilia. Antimicrob. Agents Chemother. 44, 1716–1719. [PubMed: 10817738]
33. Giacometti A, Cirioni O, Barchiesi F, and Scalise G (2000). In-vitro activity and killing effect of polycationic peptides on methicillin-resistant Staphylococcus aureus and interactions with clinically used antibiotics. Diagn. Microbiol. Infect. Dis. 38, 115–118. [PubMed: 11035243]
34. Giacometti A, Cirioni O, Del Prete MS, Paggi AM, D'Errico MM, and Scalise G (2000). Combination studies between polycationic peptides and clinically used antibiotics against Gram-positive and Gram-negative bacteria. Peptides 21, 1155–1160. 10.1016/S0196-9781(00)00254-0. [PubMed: 11035200]
35. Niu M, Li X, Gong Q, Wang C, Qin C, Wang W, and Chen P (2013). Expression of 4kD scorpion defensin and its in vitro synergistic activity with conventional antibiotics. World J. Microbiol. Biotechnol. 29, 281–288. 10.1007/s11274-012-1181-4. [PubMed: 23054701]
36. Yenugu S, and Narmadha G (2010). The human male reproductive tract antimicrobial peptides of the HE2 family exhibit potent synergy with standard antibiotics. J. Pept. Sci. 16, 337–341. 10.1002/psc.1246. [PubMed: 20552564]
37. Sánchez-Gómez S, Japelj B, Jerala R, Moriyón I, Fernández Alonso M, Leiva J, Blondelle SE, Andrä J, Brandenburg K, Lohner K, and Martínez de Tejada G (2011). Structural features governing the activity of lactoferricin-derived peptides that act in synergy with antibiotics against Pseudomonas aeruginosa in vitro and in vivo structural features governing the activity of lactoferricin-derived peptides that act in. Antimicrob. Agents Chemother. 55, 218–228. 10.1128/AAC.00904-10. [PubMed: 20956602]
38. Lin L, Nonejuie P, Munguia J, Hollands A, Olson J, Dam Q, Kumaraswamy M, Rivera H, Corriden R, Rohde M, et al. (2015). Azithromycin synergizes with cationic antimicrobial peptides to exert bactericidal and therapeutic activity against highly multidrug-resistant gram-negative bacterial pathogens. EBioMedicine 2, 690–698. 10.1016/j.ebiom.2015.05.021. [PubMed: 26288841]
39. He J, Starr CG, and Wimley WC (2015). A lack of synergy between membrane-permeabilizing cationic antimicrobial peptides and conventional antibiotics. Biochim. Biophys. Acta 1848, 8–15. 10.1016/j.bbamem.2014.09.010. [PubMed: 25268681]
40. Ulvatne H, Karoliussen S, Stiberg T, Rekdal Ø, and Svendsen JS (2001). Short antibacterial peptides and erythromycin act synergically against Escherichia coli. J. Antimicrob. Chemother. 48, 203–208. [PubMed: 11481289]
41. LeBel M (1988). Ciprofloxacin: Chemistry, mechanism of action, resistance, antimicrobial spectrum, pharmacokinetics, clinical trials, and adverse reactions. Pharmacotherapy 8, 3–33. 10.1002/j.1875-9114.1988.tb04058.x. [PubMed: 2836821]
42. Torres MDT, Voskian S, Brown P, Liu A, Lu TK, Hatton TA, and de la Fuente-Nunez C (2021). Coatable and resistance-proof ionic liquid for pathogen eradication. ACS Nano 15, 966–978. 10.1021/acsnano.0c07642. [PubMed: 33438392]
43. Crane JK, Cheema MB, Olyer MA, and Sutton MD (2018). Zinc blockade of SOS response inhibits horizontal transfer of antibiotic resistance genes in enteric bacteria. Front. Cell. Infect. Microbiol. 8, 410–412. 10.3389/fcimb.2018.00410. [PubMed: 30519543]
44. Rehman A, Patrick WM, and Lamont IL (2019). Mechanisms of ciprofloxacin resistance in Pseudomonas aeruginosa : new approaches to an old problem. J. Med. Microbiol. 68, 1–10. 10.1099/jmm.0.000873. [PubMed: 30605076]
45. Jolivet-gougeon A, and Bonnaure-mallet M (2014). Drug resistance Biofilms as a mechanism of bacterial resistance. Drug Discov. Today Technol. 11, 49–56. 10.1016/j.ddtec.2014.02.003. [PubMed: 24847653]

46. Angst DC, Tepekule B, Sun L, Bogos B, and Bonhoeffer S (2021). Comparing treatment strategies to reduce antibiotic resistance in an in vitro epidemiological setting. Proc. Natl. Acad. Sci. USA 118, 1–7. 10.1073/pnas.2023467118/-/DCSupplemental.y.
47. Wu M, Maier E, Benz R, and Hancock RE (1999). Mechanism of interaction of different classes of cationic antimicrobial peptides with planar bilayers and with the cytoplasmic membrane of Escherichia coli. Biochemistry 38, 7235–7242. 10.1021/bi9826299. [PubMed: 10353835]
48. El Solh AA, Akinnusi ME, Wiener-Kronish JP, Lynch SV, Pineda LA, and Szarpa K (2008). Persistent infection with Pseudomonas aeruginosa in ventilator-associated pneumonia. Am. J. Respir. Crit. Care Med. 178, 513–519. 10.1164/rccm.200802-239OC. [PubMed: 18467510]
49. Newman JW, Floyd RV, and Fothergill JL (2017). The contribution of Pseudomonas aeruginosa virulence factors and host factors in the establishment of urinary tract infections. FEMS Microbiol. Lett. 364. 10.1093/femsle/fnx124.
50. Yeung CK, and Lee KH (1998). Community acquired fulminant Pseudomonas infection of the gastrointestinal tract in previously healthy infants. J. Paediatr. Child Health 34, 584–587. 10.1046/j.1440-1754.1998.00290.x. [PubMed: 9928656]
51. Nagoba B, Davane M, Gandhi R, Wadher B, Suryawanshi N, and Selkar S (2017). Treatment of skin and soft tissue infections caused by Pseudomonas aeruginosa−a review of our experiences with citric acid over the past 20 years. Wound Med 19, 5–9. 10.1016/j.wndm.2017.09.005.
52. Stefani S, Campana S, Cariani L, Carnovale V, Colombo C, Lleo MM, Iula VD, Minicucci L, Morelli P, Pizzamiglio G, and Taccetti G (2017). Relevance of multidrug-resistant Pseudomonas aeruginosa infections in cystic fibrosis. Int. J. Med. Microbiol. 307, 353–362. 10.1016/j.ijmm.2017.07.004. [PubMed: 28754426]
53. Chen C, Mangoni ML, and Di YP (2017). In vivo therapeutic efficacy of frog skin-derived peptides against Pseudomonas aeruginosa-induced pulmonary infection. Sci. Rep. 7, 8548. 10.1038/s41598-017-08361-8. [PubMed: 28819175]
54. Fanos V, and Cataldi L (2001). Renal transport of antibiotics and nephrotoxicity: a review. J. Chemother. 13, 461–472. 10.1179/joc.2001.13.5.461. [PubMed: 11760211]
55. Casares D, Escrib PV, and Rosselló CA (2019). Membrane lipid composition : effect on membrane and organelle structure , function and compartmentalization and therapeutic avenues. Int. J. Mol. Sci. 20, 1–30.
56. Glukhov E, Stark M, Burrows LL, and Deber CM (2005). Basis for selectivity of cationic antimicrobial peptides for bacterial versus mammalian membranes. J. Biol. Chem. 280, 33960–33967. 10.1074/jbc.M507042200. [PubMed: 16043484]
57. Cardoso MH, Orozco RQ, Rezende SB, Rodrigues G, Oshiro KGN, Cândido ES, and Franco OL (2019). Computer-aided design of antimicrobial peptides: are we generating effective drug candidates? Front. Microbiol. 10, 3097. 10.3389/fmicb.2019.03097.
58. Pane K, Cafaro V, Avitabile A, Torres MDT, Vollaro A, De Gregorio E, Catania MR, Di Maro A, Bosso A, Gallo G, et al. (2018). Identification of novel cryptic multifunctional antimicrobial peptides from the human stomach enabled by a computational-experimental platform. ACS Synth. Biol. 7, 2105–2115. 10.1021/acssynbio.8b00084. [PubMed: 30124040]
59. Porto WF, Irazazabal L, Alves ESF, Ribeiro SM, Matos CO, Pires ÁS, Fensterseifer ICM, Miranda VJ, Haney EF, Humblot V, et al. (2018). In silico optimization of a guava antimicrobial peptide enables combinatorial exploration for peptide design. Nat. Commun. 9, 1490. 10.1038/s41467-018-03746-3. [PubMed: 29662055]
60. Kim SC, Kim DW, Shim YH, Bang JS, Oh HS, Wan Kim S, and Seo MH (2001). In vivo evaluation of polymeric micellar paclitaxel formulation : toxicity and efficacy. J. Contr. Release 72, 191–202.
61. Talbot SR, Biernot S, Bleich A, van Dijk RM, Ernst L, Hä ger C, Helgers SOA, Koegel B, Koska I, Kuhla A, et al. (2020). Defining body-weight reduction as a humane endpoint : a critical appraisal. Lab. Anim. 54, 99–110. 10.1177/0023677219883319. [PubMed: 31665969]
62. LaMotte RH, Shimada SG, and Sikand P (2011). Mouse models of acute, chemical itch and pain in humans. Exp. Dermatol. 20, 778–782. 10.1111/j.1600-0625.2011.01367.x. [PubMed: 21929688]
63. Shimada SG, and LaMotte RH (2008). Behavioral differentiation between itch and pain in mouse. Pain 139, 681–687. 10.1016/j.pain.2008.08.002. [PubMed: 18789837]

64. Jamshaid H, Din FU, Malik M, Mukhtiar M, Choi HG, Ur-Rehman T, and Khan GM (2022). A cutback in Imiquimod cutaneous toxicity; comparative cutaneous toxicity analysis of Imiquimod nanotransethosomal gel with 5% marketed cream on the BALB/c mice. Sci. Rep. 12, 14244. 10.1038/s41598-022-18671-1. [PubMed: 35987944]

65. Mekonnen A, Tesfaye S, Christos SG, Dires K, Zenebe T, Zegeye N, Shiferaw Y, and Lulekal E (2019). Evaluation of skin irritation and acute and subacute oral toxicity of lavandula angustifolia essential oils in rabbit and mice. J. Toxicol. 2019, 5979546. 10.1155/2019/5979546.

66. Siddique MI, Katas H, Amin MCI, Ng SF, Zulfakar MH, Buang F, Jamil A, and Jamil A (2015). Minimization of local and systemic adverse effects of topical glucocorticoids by nanoencapsulation : in vivo safety of hydrocortisone – hydroxytyrosol loaded chitosan nanoparticles. J. Pharmaceut. Sci. 104, 4276–4286. 10.1002/jps.24666.

67. Fensterseifer ICM, Felício MR, Alves ESF, Cardoso MH, Torres MDT, Matos CO, Silva ON, Lu TK, Freire MV, Neves NC, et al. (2019). Selective antibacterial activity of the cationic peptide PaDBS1R6 against Gram-negative bacteria. Biochim. Biophys. Acta Biomembr. 1861, 1375–1387. 10.1016/j.bbamem.2019.03.016. [PubMed: 30926365]

68. de la Fuente-Núñez C, Reffuveille F, Fernández L, and Hancock REW (2013). Bacterial biofilm development as a multicellular adaptation: antibiotic resistance and new therapeutic strategies. Curr. Opin. Microbiol. 16, 580–589. 10.1016/j.mib.2013.06.013. [PubMed: 23880136]

69. Lewis RJ, and Garcia ML (2003). Therapeutic potential of venom peptides. Nat. Rev. Drug Discov. 2, 790–802. 10.1038/nrd1197. [PubMed: 14526382]

70. Parente AMS, Daniele-silva A, Furtado AA, Melo MA, Lacerda AF, Queiroz M, Moreno C, Santos E, Rocha HAO, Barbosa EG, et al. (2018). Analogs of the scorpion venom peptide stigmurin : structural assessment , toxicity , and increased antimicrobial activity. Toxins 10, 161. 10.3390/toxins10040161. [PubMed: 29670004]

71. Lum KY, Tay ST, Le CF, Lee VS, Sabri NH, Velayuthan RD, Hassan H, and Sekaran SD (2015). Activity of novel synthetic peptides against Candida albicans. Sci. Rep. 5, 9657. 10.1038/srep09657. [PubMed: 25965506]

72. Matsuzaki K, Nakamura A, Murase O, Sugishita K, Fujii N, and Miyajima K (1997). Modulation of magainin 2 - lipid bilayer interactions by peptide charge. Biochemistry 36, 2104–2111. [PubMed: 9047309]

73. Conlon JM, Galadari S, Raza H, and Condamine E (2008). Design of potent, nontoxic antimicrobial agents based upon the naturally occurring frog skin peptides , ascaphin-8 and peptide XT-7. Chem. Biol. Drug Des. 72, 58–64. 10.1111/j.1747-0285.2008.00671.x. [PubMed: 18554256]

74. Wiegand I, Hilpert K, and Hancock REW (2008). Agar and broth dilution methods to determine the minimal inhibitory concentration (MIC) of antimicrobial substances. Nat. Protoc. 3, 163–175. 10.1038/nprot.2007.521. [PubMed: 18274517]

75. Hancock RE, and Wong PG (1984). Compounds which increase the permeability of the Pseudomonas aeruginosa outer membrane. Antimicrob. Agents Chemother. 26, 48–52. 10.1128/aac.26.1.48. [PubMed: 6433788]

76. Zhang L, Dhillon P, Yan H, Farmer S, and Hancock RE (2000). Interactions of bacterial cationic peptide antibiotics with outer and cytoplasmic membranes of Pseudomonas aeruginosa. Antimicrob. Agents Chemother. 44, 3317–3321. 10.1128/AAC.44.12.3317-3321.2000. [PubMed: 11083634]

77. Lai X, Han ML, Ding Y, Chow SH, Le Brun AP, Wu CM, Bergen PJ, Jiang JH, Hsu HY, Muir BW, et al. (2022). A polytherapy based approach to combat antimicrobial resistance using cubosomes. Nat. Commun. 13, 343. 10.1038/s41467-022-28012-5. [PubMed: 35039508]

78. Han SM, Kim JM, Hong IP, Woo SO, Kim SG, Jang HR, and Pak SC (2016). Antibacterial activity and antibiotic-enhancing effects of honeybee venom against methicillin-resistant staphylococcus aureus. Molecules 21. 79–9. 10.3390/molecules21010079. [PubMed: 26771592]

79. Odds FC (2003). Synergy, antagonism, and what the chequerboard puts between them. J. Antimicrob. Chemother. 52, 1. 10.1093/jac/dkg301. [PubMed: 12805255]

80. Pirtskhalava M, Amstrong AA, Grigolava M, Chubinidze M, Alimbarashvili E, Vishnepolsky B, Gabrielian A, Rosenthal A, Hurt DE, and Tartakovsky M (2021). DBAASP v3: database of

antimicrobial/cytotoxic activity and structure of peptides as a resource for development of new therapeutics. Nucleic Acids Res. 49, D288–D297. 10.1093/nar/gkaa991. [PubMed: 33151284]

Author Manuscript

Author Manuscript

Author Manuscript

Highlights

- Structure-function-guided design yielded peptide antibiotics with potent activity
- Ala-Scan and lysine substitutions revealed antimicrobial hotspots
- Net charge was shown as the most relevant feature for antimicrobial activity

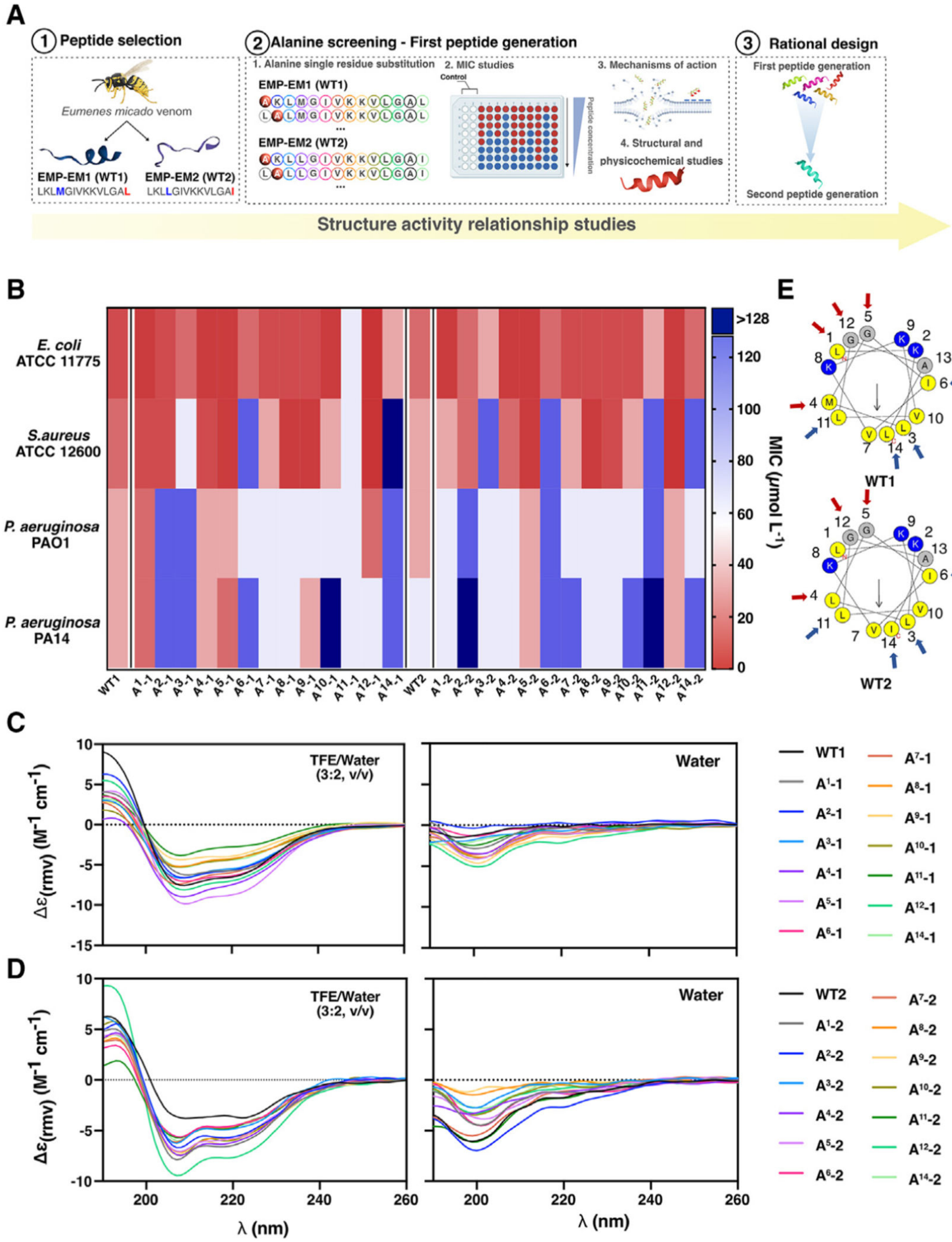

Figure 1. Design, antimicrobial activity, and secondary structure elucidation of peptides from wasp venom

(A) Schematic representation of the structure-function relationship studies, from the selection of the templates (EMP-EM1 [WT1] and EMP-EM2 [WT2]), isolated from the venom of the solitary wasp *Eumenes micado*, to the design of an optimized second-generation peptide.

(B) Antimicrobial activity of WT1 and WT2 and Ala-Scan analogs for the four pathogenic bacterial strains tested in this study. The red color represents bacterial growth inhibition, and the blue color represents bacterial growth.

(C and D) CD spectra of WT1 (C) and WT2 (D) and their respective Ala-Scan derivatives at 50 μmol L^{-1} in TFE:water 3:2 v/v and water showing the conformational transition of the peptides from random coil in water to α helix in TFE:water. CD spectra were recorded in three replicates at 25°C, using a quartz cuvette with 1-mm path length, between 260 and 190 nm at 50 nm min^{-1}, with a bandwidth of 0.5 nm.

(E) Bidimensional helical wheel representations of the wild-type peptides WT1 and WT2, indicating positions where Ala-substitution decreased (blue arrows) or enhanced (red arrows) activity.

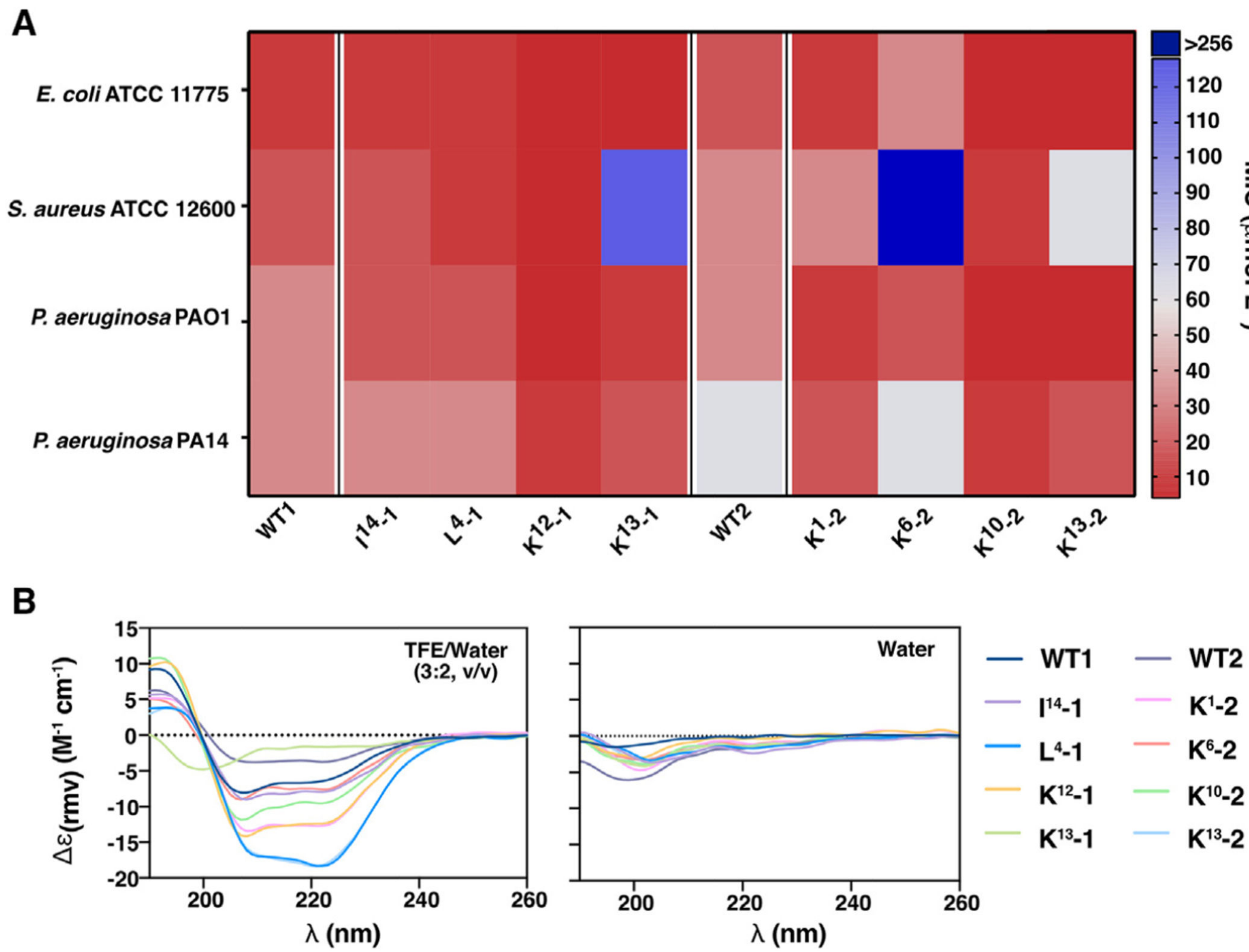

Figure 2. Antimicrobial activity and elucidation of secondary structure

(A) Antimicrobial activity of WT1, WT2, and second-generation analogs for all tested pathogenic bacteria. The red color represents bacterial growth inhibition, and the blue color represents bacterial growth. Heat maps obtained directly from OD measurements of 96-well plates after treatment are shown in Figure S4.

(B) CD spectra of WT1 and WT2 and their respective second-generation derivatives at 50 μmol L^{-1} in TFE:water 3:2 v/v, showing α helix conformation, and in water, showing random-coil conformation. CD spectra were recorded in three replicates at 25°C, using a quartz cuvette with 1-mm path length, between 260 and 190 nm at 50 nm min^{-1}, with a bandwidth of 0.5 nm.

Author Manuscript
Author Manuscript
Author Manuscript

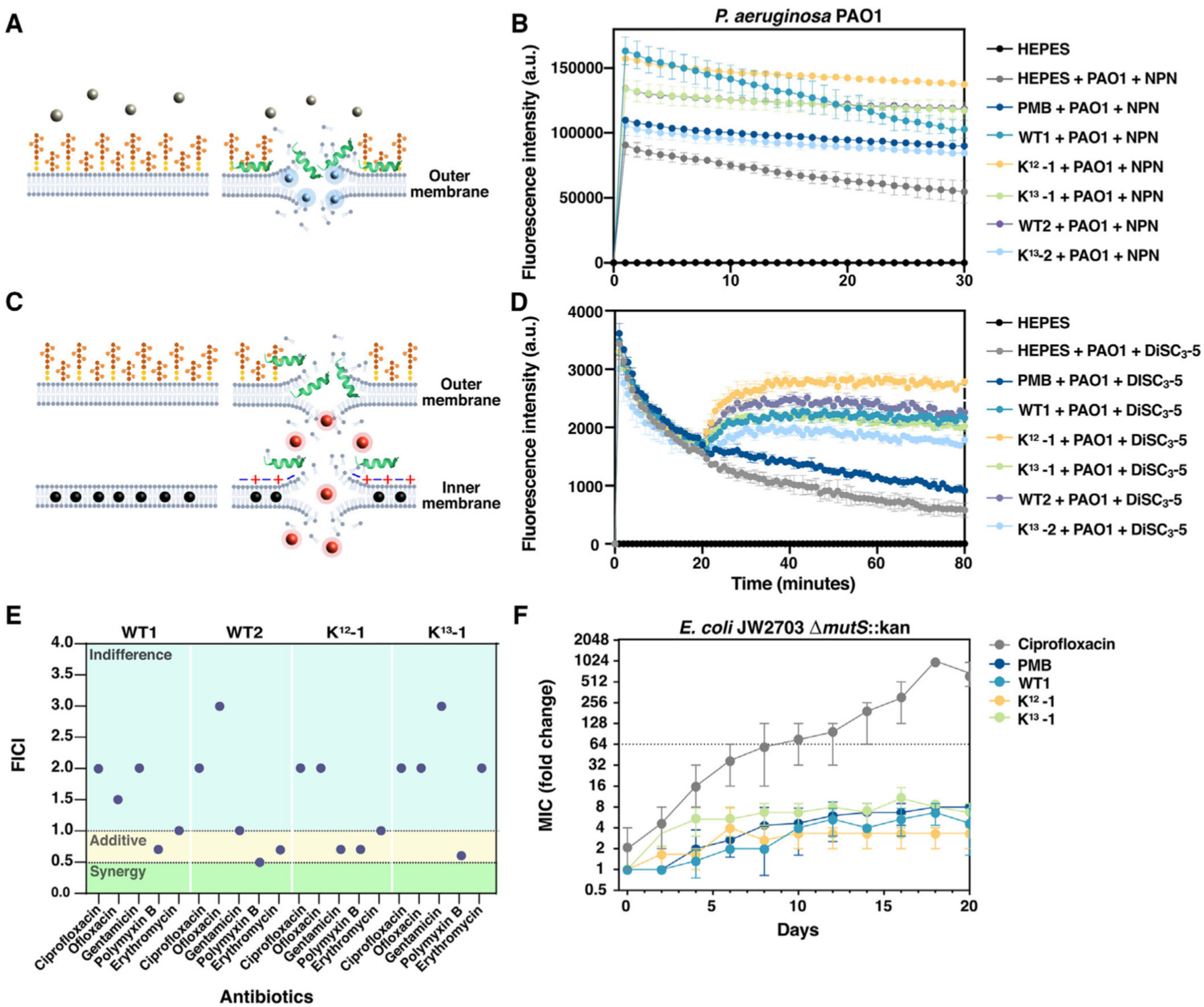

Figure 3. Mechanism of action, synergy, and bacterial resistance

(A) Schematic representation of the NPN assay, in which molecules of NPN (represented by gray spheres) present weak fluorescence emission intensity in an aqueous environment. When the outer membranes are permeabilized by peptides, the NPN molecules interact with the lipidic environment of damaged outer membranes and the intensity of blue fluorescence emission increases (represented by blue spheres).

(B) NPN graph for outer membrane permeabilization of *Pseudomonas aeruginosa* PAO1 by polymyxin B (PMB), WT1, K^{12}-1, K^{13}-1, WT2, and K^{13}-2 peptides. Profiles with a rapid increase in fluorescence emission intensity, followed by a slow decay, were obtained after measurement of white 96-well plates on a Thermo Scientific Varioskan LUX fluorescence spectrophotometer, with the excitation wavelength set to 350 nm and the emission wavelength set to 420 nm, according to the experimental procedure described in the section “experimental procedures.” All NPN assays were done in three replicates, including the controls, which consisted of only HEPES solution, HEPES solution and NPN (not shown), HEPES solution and *P. aeruginosa* PAO1 (not shown), and HEPES solution with both *P. aeruginosa* PAO1 and NPN. Data are represented as mean ± SD.

(C) Schematic representation of the $DiSC_3$-5 assay, in which molecules of $DiSC_3$-5 (represented by gray spheres) accumulate in cytoplasmic membranes and aggregate at high concentrations, causing fluorescence quenching. When the cytoplasmic membrane is destabilized by peptides, $DiSC_3$-5 migrates to the cytoplasm or to the external environment, and red fluorescence emission intensity (represented by red spheres) increases.

(D) $DiSC_3$-5 graph for cytoplasmic membrane depolarization of *P. aeruginosa* PAO1 by PMB, WT1, K^{12}-1, K^{13}-1, WT2, and K^{13}-2 peptides. Profiles with increases and decreases in fluorescence emission intensity were obtained after measurement of black 96-well plates on a Thermo Scientific Varioskan LUX fluorescence spectrophotometer, with the excitation wavelength set to 622 nm and emission wavelength set to 670 nm as described in the section "experimental procedures." $DiSC_3$-5 graph obtained after the addition of triton solution is shown in Figure S5. All $DiSC_3$-5 assays were done in three replicates, including the controls, which consisted of only HEPES solution, and HEPES solution containing PAO1 and $DiSC_3$-5. Data are represented as mean ± SD.

(E) Synergy assay for activity against *P. aeruginosa* PAO1 between ciprofloxacin, ofloxacin, gentamicin, polymyxin B, or erythromycin, and each of four peptides: WT1, WT2, K^{12}-1, and K^{13}-1. The Fractional Inhibitory Concentration Index (FICI) values, which indicate the degree of synergy between two antimicrobial agents against a target microorganism, were calculated based on the MICs of WT1, WT2, K^{12}-1, and K^{13}-1 and the commercial antibiotics used alone and in combination. FICI values <0.5 indicate synergy; $0.5 < \text{FICI} < 1$ indicates additive effects; $1 < \text{FICI} < 4$ indicates indifference; and $\text{FICI} > 4$ indicates antagonism (not represented in the graph).

(F) Resistance assay: development of resistance to ciprofloxacin, PMB, WT1, K^{12}-1, and K^{13}-1 in *Escherichia coli* Δ*mutS*. The experiment was performed for 20 days as described in detail in the section "experimental procedures." Data are represented as mean ± SD.

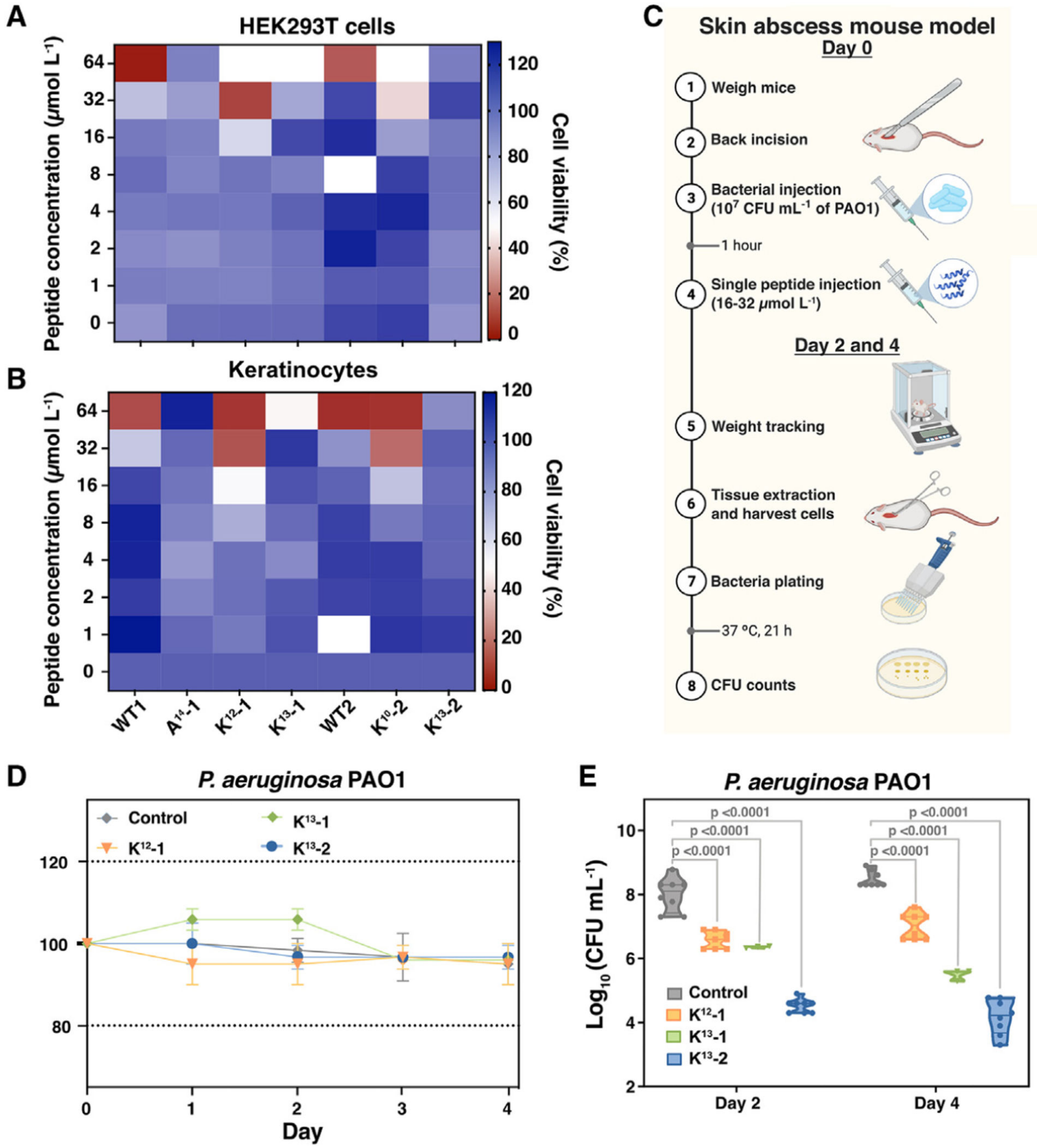

Figure 4. Cytotoxicity and *in vivo* studies

(A and B) Cytotoxic activity of WT1, A^{14}-1, K^{12}-1, K^{13}-1, WT2, K^{10}-2, and K^{13}-2 against (A) human embryonic kidney cells (HEK293T) and (B) primary human keratinocytes.

(C) Schematic representation of the *in vivo* assay procedure. The mice were anesthetized with isoflurane and weighed; their backs were shaved, and a superficial linear skin abrasion was made using a needle to damage the stratum corneum and upper layer of the epidermis. Then 50 μL of 10^7 CFU mL^{-1} in phosphate-buffered saline (PBS) of *P. aeruginosa* PAO1 was inoculated over the scratch in the back of the mice. After 1 h, peptide solutions in PBS at 32 µmol L^{-1} for K^{13}-2 and 16 µmol L^{-1} for K^{12}-1 and K^{13}-1 were added to the infected area. This procedure was done for four mice per peptide tested. After 2 days, mice from each group were killed and weighed, and the area of scarified skin was cut, homogenized using a bead beater for 20 min (25 Hz), and serially diluted for CFU quantification. This procedure was repeated after 4 days with the mice from each group. Two technical replicates were performed for each sample to ensure accuracy.

(D) Mice weight monitoring for potential *in vivo* toxicity assessment. The body weight of infected mice was normalized by the body weight of uninfected mice. Data are represented as mean ± SD.

(E) Anti-infective activity of K^{12}-1, K^{13}-1, and K^{13}-2 *in vivo* compared with control groups. Statistical significance was determined using one-way ANOVA followed by Dunnett's test; p values are shown in the graph.

Table 1.

Amino acid sequence, theoretical values of normalized hydrophobicity, normalized hydrophobic moment, net charge, ratio of polar/non-polar amino acid residues, propensity to *in vitro* aggregation, amphiphilicity index, and values of helical fraction in water and in a mixture 3:2 of TFE and water, for WT1, WT2, and their corresponding Ala-Scan analogs

Peptides		Physicochemical properties						Helical fraction	
Code	Sequence	<H>	<μH>	q	P/N	*In vitro* aggregation	Amphiphilicity index	f_H (water)	f_H (TFE:water)
WT1	LKLMGIVKKVLGAL	−0.39	0.40	4	0.56	15.42	0.79	0.05	0.34
A1–1	AKLMGIVKKVLGAL	−0.36	0.42	4	0.56	15.37	0.79	0.05	0.32
A2–1	LALMGIVKKVLGAL	−0.54	0.33	3	0.40	27.36	0.52	0.04	0.29
A3–1	LKAMGIVKKVLGAL	−0.36	0.37	4	0.56	13.64	0.79	0.07	0.29
A4–1	LKLAGIVKKVLGAL	−0.39	0.40	4	0.56	14.93	0.79	0.05	0.38
A5–1	LKLMAIVKKVLGAL	−0.40	0.39	4	0.40	29.98	0.79	0.09	0.44
A6–1	LKLMGAVKKVLGAL	−0.34	0.40	4	0.56	13.64	0.79	0.05	0.33
A7–1	LKLMGIAKKVLGAL	−0.36	0.37	4	0.56	13.65	0.79	0.09	0.31
A8–1	LKLMGIVAKVLGAL	−0.54	0.37	3	0.40	34.40	0.52	0.08	0.24
A9–1	LKLMGIVKAVLGAL	−0.54	0.29	3	0.40	56.15	0.52	0.11	0.22
A10–1	LKLMGIVKKALGAL	−0.36	0.38	4	0.56	2.75	0.79	0.09	0.23
A11–1	LKLMGIVKKVAGAL	−0.36	0.38	4	0.56	3.86	0.79	0.07	0.16
A12–1	LKLMGIVKKVLAAL	−0.40	0.39	4	0.40	102.82	0.79	0.13	0.35
A14–1	LKLMGIVKKVLGAA	−0.36	0.37	4	0.56	3.84	0.79	0.05	0.25
WT2	LKLLGIVKKVLGAI	−0.45	0.43	4	0.56	34.76	0.79	0.10	0.23
A1–2	AKLLGIVKKVLGAI	−0.41	0.45	4	0.56	34.49	0.79	0.10	0.33
A2–2	LALLGIVKKVLGAI	−0.60	0.35	3	0.40	85.50	0.52	0.15	0.29
A3–2	LKALGIVKKVLGAI	−0.41	0.41	4	0.56	27.74	0.79	0.06	0.26
A4–2	LKLAGIVKKVLGAI	−0.41	0.42	4	0.56	27.89	0.79	0.08	0.31
A5–2	LKLLAIVKKVLGAI	−0.46	0.42	4	0.40	94.76	0.79	0.10	0.30
A6–2	LKLLGAVKKVLGAI	−0.39	0.44	4	0.56	27.13	0.79	0.10	0.24
A7–2	LKLLGIAKKVLGAI	−0.41	0.40	4	0.56	27.10	0.79	0.08	0.24
A8–2	LKLLGIVAKVLGAI	−0.60	0.41	3	0.40	83.03	0.52	0.06	0.29
A9–2	LKLLGIVKAVLGAI	−0.60	0.31	3	0.40	108.91	0.52	0.06	0.31
A10–2	LKLLGIVKKALGAI	−0.41	0.41	4	0.56	10.16	0.79	0.06	0.31
A11–2	LKLLGIVKKVAGAI	−0.41	0.41	4	0.56	12.38	0.79	0.11	0.25
A12–2	LKLLGIVKKVLAAI	−0.46	0.43	4	0.40	177.88	0.79	0.08	0.38
A14–2	LKLLGIVKKVLGAA	−0.39	0.38	4	0.56	10.31	0.79	0.07	0.24

<H>, normalized hydrophobicity; <μH>, normalized hydrophobic moment; q, net charge; P/N, ratio of polar/non-polar amino acid residues; f_H, helical fraction.

Author Manuscript

Author Manuscript

Author Manuscript

Table 2.

Properties of peptides WT1, WT2, and their corresponding second-generation analogs

Peptides		**Physicochemical properties**						**Helical fraction**	
Code	**Sequence**	**<H>**	**<μH>**	**q**	**P/N**	***In vitro* aggregation**	**Amphiphilicity index**	f_H **(water)**	f_H **(TFE:water)**
WT1	LKLMGIVKKVLGAL	−0.39	0.40	4	0.56	15.42	0.79	0.05	0.34
I14–1	LKLMGIVKKVLGAI	−0.42	0.42	4	0.56	28.33	0.79	0.19	0.41
L4–1	LKLLGIVKKVLGAL	−0.42	0.41	4	0.56	21.87	0.79	0.14	0.88
K12–1	LKLMGIVKKVLKAL	−0.25	0.53	5	0.56	1.76	1.05	0.06	0.62
K13–1	LKLMGIVKKVLGKL	−0.24	0.47	5	0.75	1.77	1.05	0.14	0.13
WT2	LKLLGIVKKVLGAI	−0.45	0.43	4	0.56	34.76	0.79	0.10	0.23
K1–2	KKLLGIVKKVLGAI	−0.26	0.57	5	0.75	31.51	1.05	0.12	0.62
K6–2	LKLLGKVKKVLGAI	−0.24	0.48	5	0.75	26.61	1.05	0.10	0.41
K10–2	LKLLGIVKKKLGAI	−0.26	0.35	5	0.75	8.22	1.05	0.14	0.50
K13–2	LKLLGIVKKVLGKI	−0.29	0.51	5	0.75	8.15	1.05	0.15	0.89

Theoretical values of: normalized hydrophobicity (<H>); normalized hydrophobic moment (<μH>); net charge (q); ratio of polar/non-polar amino acid residues (P/N); propensity to aggregate *in vitro;* amphiphilicity index; and values of helical fraction (f_H) in water and in a mixture 3:2 of TFE and water.